NAVAL AIR WARFARE CENTER AIRCRAFT DIVISION
PATUXENT RIVER, MARYLAND

TECHNICAL REPORT

REPORT NO: NAWCADPAX--97-255-TR

COPY NO. _____

ADVANCED COMPUTATIONAL MODEL FOR ROCKET PLUME EFFECTS ON ESCAPE SYSTEM AERODYNAMIC CHARACTERISTICS

2 June 1997

Approved for public release; distribution is unlimited.

REPORT DOCUMENTATION PAGE

Form Approved
OMB No. 0704-0188

1. AGENCY USE ONLY *(LEAVE BLANK)*	2. REPORT DATE	3. REPORT TYPE AND DATES COVERED
	2 June 1997	

4. TITLE AND SUBTITLE

Advanced Computational Model for Rocket Plume Effects on Escape System Aerodynamic Characteristics

5. FUNDING NUMBERS

6. AUTHOR(S)

S. G. Rock
S. D. Habchi

Contract No. N62269-96-C-0027

7. PERFORMING ORGANIZATION NAME(S) AND ADDRESS(ES)

CFD Research Corporation
3325 Triana Blvd.
Huntsville, Alabama 35805

8. PERFORMING ORGANIZATION REPORT NUMBER

NAWCADPAX--97-255-TR
CFDRC Report 4806/2

9. SPONSORING/MONITORING AGENCY NAME(S) AND ADDRESS(ES)

Naval Air Warfare Center Aircraft Division
22347 Cedar Point Road Unit #6
Patuxent River, Maryland 20670-1161

10. SPONSORING/MONITORING AGENCY REPORT NUMBER

11. SUPPLEMENTARY NOTES

Technical Monitor: Thomas Marquette (Code 4.6.2.1)
Naval Air Warfare Center Aircraft Division
Patuxent River, Maryland 20670

12a. DISTRIBUTION/AVAILABILITY STATEMENT

Approved for public release; distribution is unlimited.

12b. DISTRIBUTION CODE

13. ABSTRACT *(Maximum 200 words)*

The focus of this SBIR project was to develop and adapt existing computational methodologies for three-dimensional comprehensive analysis of ejection seat aerodynamics, including rocket plume effects. This Phase I study (6 months) focused on analyzing ejection seat rocket propulsion systems and developing techniques to solve for rocket plume flows within the ejection seat environment.

Various methods were investigated for prescribing boundary and initial conditions for the seat rockets. The selected method utilizes a model that prescribes 3D nozzle exit boundary profiles extracted from detailed rocket nozzle calculations. Also, a multi-domain gridding method that allows for many-to-one interface meshing was developed and tested for efficient and accurate rocket plume resolution within the 3D ejection seat computational environment.

Basic rocket plume model validations were made to a jet-in-axial and jet-in-crossflow problems. Excellent agreement was obtained for the jet-in-axial flow and reasonable agreement was obtained for the jet-in-crossflow. Validations were also performed for the Pintle Escape propulsion system rockets. Good agreement with test data was obtained for thrust levels obtained for various pintle positions. 3D ejection seat with rocket power calculations were also made to demonstrate the feasibility of the approach and the potential use of the model.

14. SUBJECT TERMS	15. NUMBER OF PAGES
Advanced Computational Model Rocket Plume Effects	78
	16. PRICE CODE

17. SECURITY CLASSIFICATION OF REPORT	18. SECURITY CLASSIFICATION OF THIS PAGE	19. SECURITY CLASSIFICATION OF ABSTRACT	20. LIMITATION OF ABSTRACT
Unclassified	Unclassified	Unclassified	SAR

CFD Research Corporation
3325 Triana Blvd. • Huntsville, Alabama 35805 • Tel.: (205) 536-6576 • FAX: (205) 536-6590 • info@cfdrc.com

ADVANCED COMPUTATIONAL MODEL FOR ROCKET PLUME EFFECTS ON ESCAPE SYSTEM AERODYNAMIC CHARACTERISTICS

SBIR Phase I Final Report

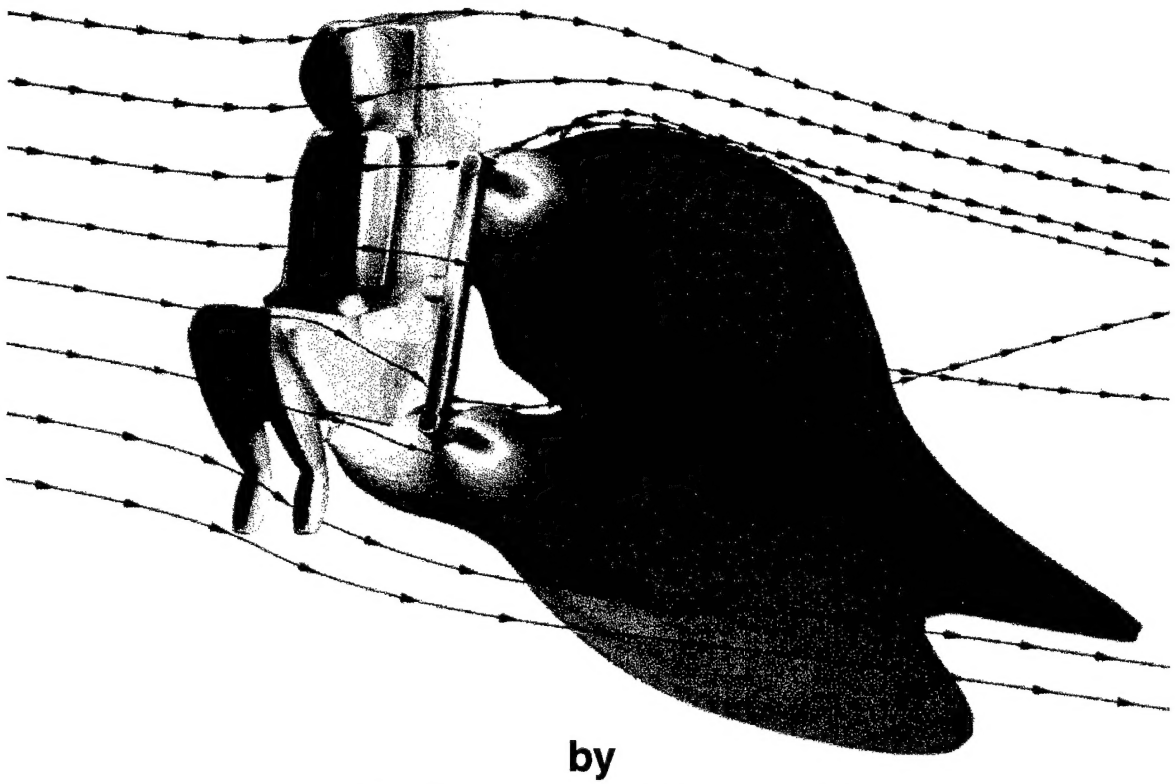

by
S.G. Rock and S.D. Habchi

prepared for
Naval Air Warfare Center - Aircraft Division
Warminster, PA 18974

R&D Services and Software for Computational Fluid Dynamics (CFD)
Branch Office: 2 Lakeview Ave., Suite 200 • Piscataway, New Jersey 08854 • Tel.: (908) 424-9393 FAX: (908) 424-9399

ADVANCED COMPUTATIONAL MODEL FOR ROCKET PLUME EFFECTS ON ESCAPE SYSTEM AERODYNAMIC CHARACTERISTICS

SBIR Phase I Final Report

CDRL Item A001

by
S.G. Rock and S.D. Habchi

June 1996

CFDRC Report: 4806/2

prepared for
Naval Air Warfare Center - Aircraft Division
Warminster, PA 18974

Contract Number: N62269-96-C-0027
Technical Monitor: T. Marquette

PREFACE

This is the final report for a Navy SBIR Phase I study entitled, "Advanced Computational Model for Rocket Plume Effects on Escape System Aerodynamic Characteristics." This project was sponsored by the US Navy , Naval Air Warfare Center - Aircraft Division (NAWC-A/D) (NAWC-A/D Contract Number: N62269-96-C-0027) and conducted by CFD Research Corporation (CFDRC) (CFDRC Project Number: 4806). The Project Manager was Sami D. Habchi and the Principal Investigator was Mr. Stacey G. Rock of CFDRC. Mr. Thomas J. Marquette was the Navy Technical Monitor.

SUMMARY

The overall objective of this SBIR project is to develop and adapt existing computational methodologies to create a computational environment for three-dimensional comprehensive analysis of ejection seat aerodynamics, including rocket plume effects. The focus of this Phase I study (6 months) was to investigate and analyze ejection seat rocket propulsion systems and develop techniques to solve for rocket plume flows within the 3D ejection seat computational environment. This report presents the findings of the Phase I study, including detailed discussions of the selected methodologies and presentation of demonstration and validation efforts.

Various methods were investigated for prescribing boundary and initial conditions for the seat rockets. The selected method utilizes a model that prescribes 3D nozzle exit boundary profiles extracted from detailed rocket nozzle calculations. Existing ejection seat analysis computational tools were adapted for rocket plume calculations. A multi-domain gridding method that allows for many-to-one interface meshing was developed and tested for efficient and accurate rocket plume resolution within the 3D ejection seat computational environment.

The developed/adapted tools were demonstrated and validated against test data. Basic validations were made for a jet-in-axial and jet-in-crossflow problems. Excellent agreement was obtained for the jet-in-axial flow and reasonable agreement was obtained for the jet-in-crossflow problem. Validations were also performed for the Pintle Escape propulsion system rockets. Good agreement with test data was obtained for thrust levels obtained for various pintle positions. 3D ejection seat with rocket power calculations were also made to demonstrate the feasibility of the approach and the potential use of the model.

The result of this Phase I effort is the development and validation of a basic rocket plume model for prediction of ejection seat rocket plume flows. The model was also loosely incorporated into the 3D ejection seat computational environment and demonstrated for 3D ejection seat plume flow predictions. In Phase II, the development and adaptation of the 3D model will be completed and an extensive validation effort will be conducted for both traditional and PEPS escape propulsion systems.

ACKNOWLEDGMENTS

The authors of this report would like to thank Dr. Anantha Krishnan of CFDRC for his support in adapting CFD-ACE to perform equilibrium simulations of ejection seat rocket plumes, and also Mr. Matt Thomas for providing information on the composition and properties of solid propellants. The active participation of the Navy Technical Monitor, Mr. Tom Marquette, has been very helpful and also appreciated. The authors also would like to thank Mr. Joe Morris and Mr. Bill Barnette of Aerojet for their full cooperation in providing detailed geometry and test data on the PEPS system. The technical guidance and advice of both Dr. Andrzej Przekwas and Dr. Ashok Singhal of CFDRC was very valuable. Ms. J. Swann was responsible for the final preparation of this report.

TABLE OF CONTENTS

		Page
PREFACE		i
SUMMARY		ii
ACKNOWLEDGEMENTS		iii
1.	INTRODUCTION	1
	1.1 Background	1
	1.1.1 Rocket Plume Effects on Seat Aerodynamics	1
	1.1.2 Escape System Computational Methodologies	3
	1.2 Phase I Objectives	3
	1.3 Phase I Results	4
2.	OVERVIEW OF EJECTION SEAT ROCKET PROPULSION SYSTEMS	6
	2.1 Fixed and Controllable Propulsion Concepts	6
	2.2 Modeling Requirements for Rocket Propulsion Systems	7
3.	COMPUTATIONAL TOOLS OVERVIEW AND ADAPTATIONS	10
	3.1 CFD-ACE Overview	10
	3.2 CFD-ACE Combustion Mechanism Adaptation	11
	3.3 CFD-ACE Controllable Propulsion Boundary Condition Adaptation	13
	3.4 CFD-ACE Local Grid Refinement Methodology Adaptations	15
4.	INVESTIGATION OF INITIAL AND BOUNDARY CONDITIONS	22
5.	BASIC PLUME MODEL VALIDATION	28
	5.1 Validation Study for a Plume in an Axial Flow	28
	5.2 Validation Study for a Plume in a Crossflow	33
6.	DEMONSTRATION AND VALIDATION FOR PEPS	37
	6.1 Discussion of PEPS Nozzle Testing by Aerojet Corporation	37
	6.2 Discussion of PEPS Nozzle Analysis by CFDRC	39
	6.3 Comparison of Measured and Computed Nozzle Thrust Profiles	47
	6.4 PEPS Plume Flow Analysis	48
	6.5 Demonstration of Plume Model Within Ejection Seat Environment	52
	6.5.1 Computational Grids	52
	6.5.2 Computational Results	55
	6.5.3 Plume Shape Predictions	58
7.	CONCLUSIONS AND RECOMMENDATIONS	64
	7.1 Accomplishments of Phase I	64
	7.2 Recommendations for Phase II	65
8.	REFERENCES	67

1. INTRODUCTION

1.1 Background

The rocket motor is an essential part of the escape system used in both ejection seats and escape capsules. The thrust level provided by the rockets helps the seat in clearing the tail of the aircraft and propels the pilot to safety. Current and future escape system technologies are expected to use multiple and variable thrust nozzles for seat propulsion and control. Wind tunnel and numerical simulations have shown that the rocket plume can significantly influence the aerodynamic behavior of the ejection seat or escape capsule especially at high angle-of-attack ejections. These effects will be compounded by the expected future use of multi-nozzle controllable propulsion seat systems. To fully understand the aerodynamic behavior of the ejection seat, which is essential for designing a safe system, the influence of the rocket plume on the aerodynamic behavior has to be well understood. Although wind tunnel testing has been extensively used to assess rocket plume influence on escape system performance, its use has been mostly limited to using cold plumes to eliminate the complexity and cost involved in using explosive rocket fuels.

1.1.1 Rocket Plume Effects on Seat Aerodynamics

Various wind tunnel tests have shown that the rocket plumes have considerable effect on the escape system aerodynamic characteristics. Wind tunnel tests conducted on the CREST seat (Reichenau, 1988) and the B 1A escape capsule (Bensen, 1971) have shown that the rocket plumes produce significant increases in the magnitude of the normal force and pitching moment coefficients. The CREST tests were conducted using a half scale ejection seat and occupant. The CREST seat incorporates two TVC rockets located at the lower aft seat corners, Figure 1-1. The rocket efflux and thrust were simulated using non-metric nozzles plumbed to the facility high pressure air supply. The rockets were simulated at modulating levels of 100-, 90-, 75-, and 50-percent full rated thrust conditions. Figure 1-2 shows comparison of the rocket-off to rocket-on data obtained at a free stream Mach number of 0.6. This figure shows that all the rocket-on thrust settings produced significant increases in the magnitude of both the normal force and pitching moment coefficients. Data obtained for higher free stream Mach numbers showed that the rocket plume effects decreased with increasing Mach number.

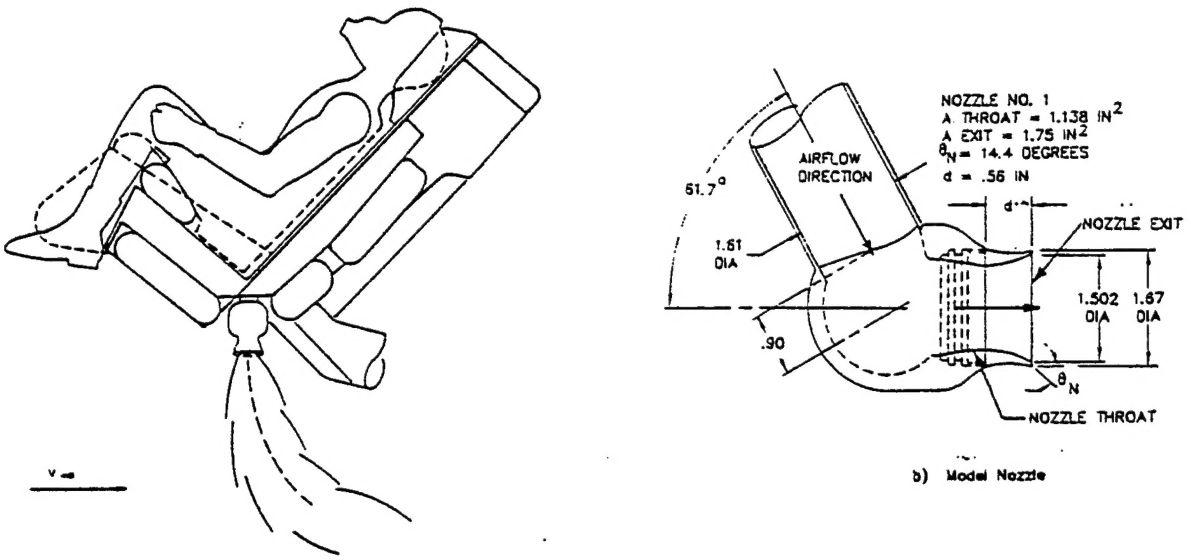

Figure 1-1. CREST Ejection Seat with Rocket Motors, (Reichenau, 1988)

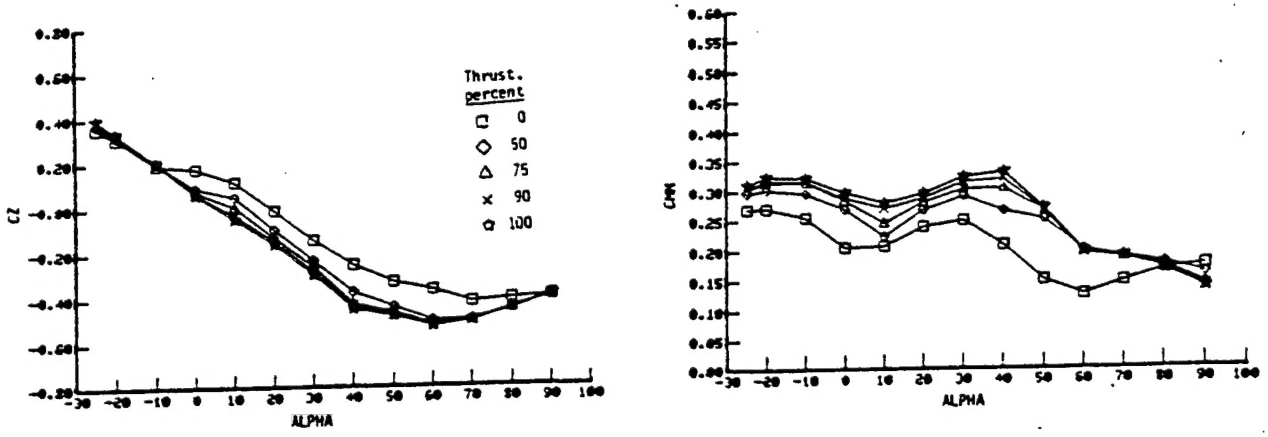

Figure 1-2. Effect of Rocket Plume Simulation on the Normal Force and Pitching Moment Coefficients of the CREST Seat; M = 0.6, β = 0 (Reichenau, 1988)

The B-1A escape capsule tests were conducted using a .036 scale B-1 escape model configuration with and without rocket power. The rocket exhaust plumes were simulated by means of high pressure nitrogen ducted to nozzles located below the module. The direct thrust of the rockets was isolated from the force balance so that only the aerodynamic interference caused by the rocket plume could be measured. The test

longitudinal data especially the lift and moment coefficients.

The reason for the rocket exhaust plume effects may be due to the increase in pressure under the seat and capsule produced by free stream flow deflecting around the rocket plumes. Also the back pressure usually decreases due to the entrainment of the rocket plume. This lower pressure results in an increase of the normal force and pitching moment coefficients. This effect is compounded when the seat or capsule is near the aircraft forebody.

The literature (Venkathapathy, 1988; Obayashi, 1988; Deiwert, 1983; Norris, 1979) shows that rocket plume flows have also significant effects on other aerospace systems such as missile aerodynamics, space shuttle aerodynamics caused by main engine and solid rocket motor plumes, and others.

1.1.2 Escape System Computational Methodologies

The U.S. Navy has been using CFD methods for the last few years to analyze the aerodynamic characteristics of ejection seats and escape capsules. The CFD simulations, unlike Wind Tunnel testing, provide detailed and complete flow field data that include the six aerodynamic coefficients used for trajectory simulations. Such data have been used to better assess the location of the pitot tubes on the NACES seat and for design requirements of various stabilization devices. The CFD tools have been extensively validated against Wind Tunnel test data (Habchi, et al., 1992; Habchi, et al., 1994; Habchi, et al., 1995; Hufford, et al., 1994; Habchi, et al., 1995a) and have proven to be accurate and reliable tools to analyze the aerodynamic behavior of escape systems. Efforts are currently underway to extend the capability of the CFD tools to handle Seat/Aircraft separation dynamics and to predict the trajectory of the jettisoned canopy. However for this CFD methodology to be complete, this capability has to be extended so that rocket plume effects can be accounted for in the aerodynamic analysis.

1.2 Phase I Objectives

The overall objective of Phase I of this program was to develop and adapt existing computational methodologies for rocket plume flow fields that are capable of predicting the effect of rocket plumes on ejection seat aerodynamic behavior. The developed methodology utilizes a rocket nozzle and plume performance computational method coupled with an existing computational environment for ejection seat flows.

The specific objectives of Phase I were:

a. Identify Ejection Seat rocket performance parameters and develop a comprehensive understanding of system operating environment.

b. Develop and adapt existing computational tools for detailed 2D axi-symmetric investigation of ejection seat rocket plume flows.

c. Validate 2D rocket plume predictions against available wind tunnel test data including those for escape systems.

d. Assess the gridding and physical modeling requirements of the full 3D simulation including seat/occupant, multi-nozzle systems with controllable propulsion.

e. Conduct preliminary calculations of 3D ejection seat flows with rocket plume effects and demonstrate feasibility of approach.

f. Develop specific recommendations for Phase II work on computational schemes for grid adaptation/refinement for capturing plume shape(s), multi-nozzle systems and controllable propulsion.

1.3 Phase I Results

All of the objectives of Phase I were successfully accomplished. A basic plume model was developed and loosely incorporated into an ejection seat computational environment. Several demonstration and validation calculations proved the feasibility and efficiency of the proposed approach. The Phase I accomplishments can be summarized as follows:

- The requisite simulation parameters, required for plume flow calculation within the ejection seat environment, were investigated, selected, and implemented for concise problem definition. A set of experimental and numerical data and methods was investigated and collected for model definition and validation.

- The Fourth Generation Pintle Escape Propulsion System (PEPS) was investigated and studied for implementation into the rocket plume model.

Several reports and test material were collected for model definition and validation.

- Initial and boundary conditions were investigated for efficient implementation into the 3D ejection seat environment. An existing boundary condition profile method was selected and validated in Phase I.

- The CFD-ACE code was adapted for basic ejection seat plume flow calculations. The adaptations include: (i) expansion of thermodynamic database; (ii) development of controllable propulsion boundary conditions and (iii) adaptation of local grid refinement methodology using the multi-domain many-to-one domain interface methodology.

- The basic capabilities of the plume model were validated against experimental data that included jet-in-axial flow and jet-in-crossflow. Excellent agreement was obtained for the jet-in-axial flow case and reasonable agreement was obtained in the jet-in-crossflow test case.

- The plume model was demonstrated and validated for PEPS. Several calculations were made with pintle at different positions. Thrust profiles were calculated for each pintle position and showed excellent agreement with test data.

- Demonstration calculations were performed for the 3D ejection seat with power-on simulation using the adapted many-to-one capability. Plume shape and aerodynamic coefficient predictions showed expected trends and proved the feasibility of the approach.

The accomplishments of Phase I prove the feasibility of the proposed approach. The proposed methodology takes advantage of and enhances existing ejection seat computational tools. Demonstration of the many-to-one local grid refinement methodology shows the capability of the method in capturing rocket plume shape and characteristics efficiently (local grid resolution), and the consistency of the method with existing ejecting seat computational methods. During Phase II, the development and adaptation of the methodologies shall be completed and extensively validated against test data.

2. OVERVIEW OF EJECTION SEAT ROCKET PROPULSION SYSTEMS

2.1 Fixed and Controllable Propulsion Concepts

Current escape systems used in military aircraft utilize solid-grain rocket propulsion. This system provides a fixed level of thrust throughout the full ejection period. During the last few years, efforts have been under way to modify this approach by introducing a propulsion system in which multiple rockets with variable thrust time profiles could be used (McDonald, 1990). This system provides fully controllable propulsion to suit the circumstances of each emergency. Such a system would not only provide a variable thrust time profile, but would also permit the propulsion system to provide stabilization, to control the forces applied on the crew member and to control the escape trajectory.

A sketch of a propulsion system that utilizes four rocket engines is shown in Figure 2-1. The four engines are arranged on the seat so that their thrust vectors are offset from the center of gravity. The overall thrust and rotational moments in pitch and yaw can be controlled simply by controlling the relative thrust of each engine. Roll moments can also be handled by skewing the thrust vectors or by adding more engines.

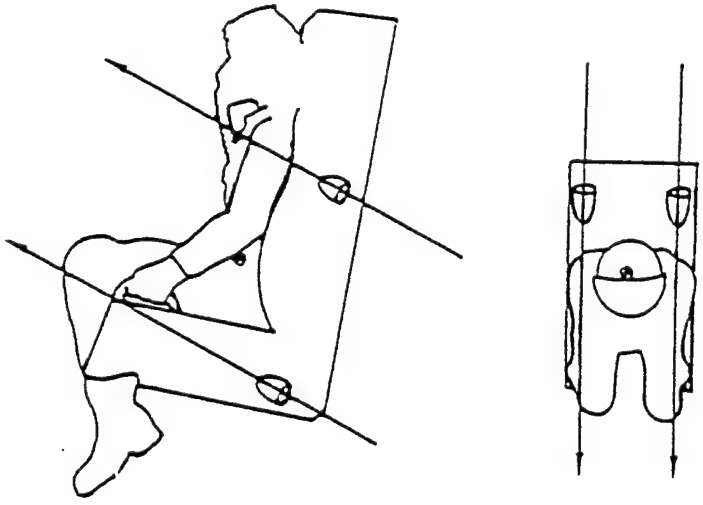

Figure 2-1. Multiple Rocket Controllable Propulsion System for a Generic Ejection Seat

2.2 Modeling Requirements for Rocket Propulsion Systems

Prior to developing and validating a comprehensive rocket plume model that takes into account all of the relevant features that affect the aerodynamic behavior of the escape system, it is essential to fully comprehend the operating requirements of rockets used for escape system operation. Through discussions with Navy engineers, it was decided that part of this Phase I effort should focus on simulating the controllable propulsion system of the 4th Generation Ejection Seat. With this focus in mind, a task was dedicated for this effort. The specific objectives of this task are:

a. perform an extensive literature review of numerical and experimental methods for simulating rocket plumes,

b. obtain a set of experimental and analytical data for validation,

c. obtain specifics on the geometry and operating conditions of the 4th Generation Ejection Seat system.

All of the above objectives were accomplished. An extensive review of the literature for nozzle, plume, and free-jet flow fields was conducted (Love, 1959; Putnam, 1981; Deiwert, 1984; Hoffmann, 1987; Venkatapathy, 1988, 1991; Obayashi, 1988; Holcomb, 1991; Ahmad, 1978; Fearn, 1978, 1979; Roth, 1989; Chiu 1993) . A variety of technical papers and journal articles was obtained that contain computational and experimental studies for plume flow fields. These studies cover three classes of problems relevant to escape system plume flow fields. The first is axial or base plume flow fields. An example of this type of flow field is a missile with a rocket plume exiting from its base. The second class of problem is a jet or plume in a crossflow. An example of this type of flow field is a Short Take-Off and Vertical Landing (STOVL) aircraft that employs a propulsive jet oriented perpendicular to the free-stream flow field. This type of plume flow field produces a complex three-dimensional interaction between the plume and the aerodynamic characteristics of the aircraft. Both of these types of flow fields can be produced by the propulsion system of ejection seats depending upon the seat attitude. The third class of problems reviewed are tests of actual escape systems (Touron, 1971; Reichenau, 1988; Salemann, 1989). A limited number of reports were obtained for ejection seat and escape capsule wind tunnel tests.

A careful review of the available literature revealed that the accurate simulation of the

aerodynamic effects of the rocket plume is based upon an accurate prediction of the plume shape and the surface pressures near the plume base (Love, 1959;Touron, 1971; Reichenau, 1988; Salemann, 1989). As a result two sets of experimental and analytical data were selected to validate the baseline rocket plume model. The first data set was taken from the data report of a Rockwell test of a 0.036 scale B-1 escape capsule (Touron, 1971). The data consist of calibration measurements of model plume shapes for the escape capsule rockets at different jet to free-stream pressure ratios. This set of data falls into the category of axial or base plume flow fields. A second set of experimental data was chosen from the works of Fearn (1978, 1979) and Roth (Roth, 1989; Chiu et al, 1993). This data set consists of measurements of plume velocity centerline and surface pressures for a subsonic jet exiting perpendicularly through a flat plate into a crossflow. These two data sets were used for validating the basic capabilities of the rocket plume model.

An additional literature review was conducted for advanced ejection seats and controllable propulsion systems. Several papers (Wheeler, 1993; Schoen, 1993; Ritland, 1994; Peterson, 1995) contained overviews of the 4th Generation Ejection Seat including the operating conditions of the Pintle Escape Propulsion System (PEPS), see Table 2-1. McDonnell Douglas Aerospace (McDonnell Douglas 1994) provided a copy of the initial test report for the PEPS program. Test data from this report were used to validate the improved rocket plume model for ejection seat operating conditions. Aerojet Corporation also provided dimensional drawings of the PEPS system that were used to create geometry and grid models of the pintle nozzle. A schematic of the PEPS system is shown in Figure 2-2. Details of the geometry creation are discussed in Section 6.2. The solid propellant for PEPS is classified as a reduced smoke, hazards class 1.3 propellant composed of ammonium-perchlorate and HTBB. However, details of the propellant composition or thermodynamic properties were not available. Therefore, the propellant properties were closely approximated using methods discussed in Section 3.2.

Table 2-1. Summary of 4th Generation Seat Propulsion System Characteristics (Ritland, 1994)

Parameter	4th Generation Escape System (PEPS)
Fuel	Ammonium Perchlorate-HTBB
Total Impulse	4500
Chamber Pressure (psi)	2500
Flame Temperature (F)	4960
Thrust/Nozzle (lbf)	150-2,500
Max System Thrust (lbf)	5000
Burn Time (sec)	1
Control Method	Proportional Pintle
Command Frequency (Hz)	>200
Estimated Weight (lbs)	85

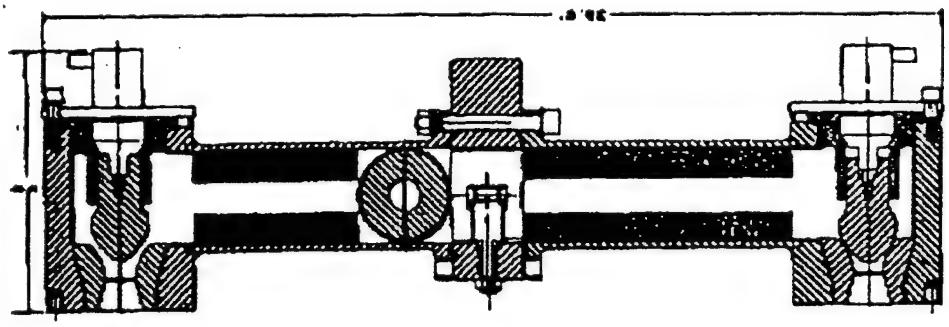

Figure 2-2. PEPS Motor Cross-Section (Wheeler, 1993)

3. COMPUTATIONAL TOOLS OVERVIEW AND ADAPTATIONS

The final product of this research effort is a CFD computational environment that is capable of predicting ejection seat aerodynamic characteristics including rocket plume effects. The starting tools for this environment are various CFD methodologies and techniques that have been developed by CFDRC, adapted for ejection seat applications and extensively used and validated for escape system application. These tools include: the geometry modeler and grid generator, CFD-GEOM; the flow solver, CFD-ACE; and the flow visualizer/post-processor, CFD-VIEW. CFD-GEOM and CFD-VIEW required no adaptation or further development for this project. CFD-ACE required some adaptation for efficient and accurate modeling of the rocket plume effects. An overview of the CFD-ACE code along with a discussion of the adaptations made in Phase I are presented below.

3.1 CFD-ACE Overview

The CFD-ACE code is a commercial CFD software that has been developed by CFDRC. The development of CFD-ACE has been greatly influenced by its application to escape system analysis. The basic capabilities of the code have been validated against several benchmark problems. The code features that are relevant to the escape system analysis have also been validated (i.e., turbulence modeling and high order differencing schemes). The CFD-ACE code has been extensively used and validated for ejection seat applications (without rocket plume effects). The salient features of CFD-ACE include:

- finite volume, multi-block structured grid flow solver for steady/unsteady, laminar/turbulent flows;
- unstructured grid flow module for complex geometric configurations;
- compressible and incompressible flows;
- combustion model with up to 40 step chemical reaction;
- various turbulence models including k-ε and RNG k-ε models;
- high order differencing schemes with shock capturing capability;
- variable properties and JANNAF standard thermodynamic tables

- advanced X/Motif GUI; and

- documentation including validation manual that includes results of validation against all major benchmark problems.

The CFD-ACE code, as seen above, has the basic capabilities to handle the ejection seat problem with plume effects. The two main areas that needed further adaptation and development for this project were:

a. updating combustion capability and thermodynamic database for escape system rocket propulsion; and

b. adapting/developing new gridding methodology that allows for local grid refinement for efficient rocket plume resolution.

The thermodynamic database has been updated under this Phase I effort for the fourth generation escape system propulsion. Further extension of the database may be needed in Phase II if other propulsion systems are considered.

Prior to this effort, one gridding capability that existed inside CFD-ACE was the multi-domain many-to-one domain interface capability. This technique allows for different grid resolutions at a domain interface which in turn would allow using a finer grid domain for the rocket plumes. This capability, however, was never tested or validated. Under this Phase I effort the many-to-one capability of CFD-ACE was debugged, tested and used for demonstration on the ejection seat with rocket plume simulation.

Details on CFD-ACE adaptation are presented below.

3.2 CFD-ACE Combustion Mechanism Adaptation

The solid propellant used in the 4th Generation Escape Systems tests was identified as a reduced smoke, hazards class 1.3 propellant composed of Ammonium-Perchlorate (AP) and HTBB. Conventional reduced smoke propellants are non-aluminized propellants. Since aluminum is not a combustion product, the need to model solid particulates was eliminated (Kruse, 1994). Therefore, the standard finite-rate and equilibrium chemistry models of CFD-ACE were sufficient for simulating the solid rocket motor nozzle and

plume. In order to perform these nozzle calculations, the combustion products generated in the combustion chamber had to be specified. These combustion products, while unknown, could be closely approximated by performing an equilibrium chemistry calculation for the rocket fuel composition at the prescribed chamber pressure. However, the actual composition (percent mass of AP and percent mass of HTBB) of the solid propellant was not specified in the available literature.

To determine the actual combustion products, a series of equilibrium computations was performed for the compositions shown in Table 3-1. By matching the nominal chamber pressure and the nominal flame temperature, a close approximation of the combustion products entering the PEPS nozzle was achieved. Case 4 most closely predicted the reported flame temperature of 4,960 F. The predicted equilibrium composition is presented in Table 3-2. Also included in Table 3-2 are the equilibrium compositions at the nozzle throat and exhaust based on a one-dimensional, isentropic expansion to one atmosphere.

Table 3-1. Equilibrium Chemistry Computations for the Combustion Chamber

Case #	Percent AP	Percent HTBB	Chamber Press. (psi)	Flame Temp. (F)
1	84	16	2500	4486
2	85	15	2500	4677
3	86	14	2500	4832
4	87	13	2500	4981
5	88	12	2500	5091

The thermodynamic database for CFD-ACE previously contained twenty five species: CH_3, CH_4, C_2H_4, C_3H_6, C_3H_8, C_7H_{16}, $C_{10}H_{19}$, CH_6N_2, CO, CO_2, H_2, O_2, N_2, H_2O, HCN, OH, H, O, N, NO, NO_2, N_2O_4, N_2H_4, AR, HE. Based on the compositions presented in Table 3-2, the species HCL and CL were added to the thermodynamic and transport property database of CFD-ACE. The thermodynamic and transport properties of the additional species were taken from the report of McBride, et al. (1993).

Table 3-2. Equilibrium Mass Fractions for Case 4

Species	Chamber	Throat	Ambient
H2O	0.2819	0.28265	0.2518
HCL	0.26068	0.26419	0.26999
CO2	0.19459	0.20167	0.28473
CO	0.13754	0.13305	0.08019
N2	0.10446	0.10476	0.10498
CL	0.00898	0.00561	0
H2	0.00478	0.00479	0.00831
other	0.00106	0.00328	0

3.3 CFD-ACE Controllable Propulsion Boundary Condition Adaptation

The addition of multiple rockets with controllable propulsion adds a level of complexity to the basic ejection seat computational environment. In general, the processes to be modeled are unsteady and require transient flow solutions. In addition, the simulation of multiple rockets that are fired independently requires thrust time histories for each rocket. In the computational environment, these thrust time histories take the form of time varying nozzle exhaust boundary conditions. To maximize the efficiency of these transient simulations, a nozzle exhaust boundary condition has been developed for this project that can efficiently simulate multiple rockets with varying thrust. This new nozzle exhaust boundary condition was incorporated into the CFD-ACE ejection seat computing environment by the addition of a new subroutine. This subroutine operates by applying axisymmetric nozzle exhaust profiles at nozzle exits in the 3D seat environment. This methodology of solving for the nozzle flowfield and the plume flowfield separately was validated in Phase I (see Section 4).

This routine is particularly flexible because a series of boundary condition files can be created that model different thrust levels. In this manner, the thrust of each rocket nozzle in the 3D environment can be controlled individually and as a function of time. To illustrate the use of this new boundary condition routine, the following example is presented. To model a pitch maneuver similar to the initial Aerojet test discussed in Section 6.1, a thrust control input file similar to Table 3-3 is created. This table contains a thrust time history for each nozzle in the form of commanded pintle positions. These

commanded pintle positions are indexed to a series of axisymmetric pintle nozzle solutions and associated nozzle exit boundary conditions to control the transient simulation of the rocket nozzles. A series of such axisymmetric solutions is presented in Section 6.4.

The actual nozzle exhaust boundary conditions are specified by accessing the database of nozzle exhaust profiles. For each axisymmetric nozzle solution, an input file similar in structure to Table 3-4 is created. This file contains information about the radius of the nozzle exit, its orientation in the 3D environment, and nozzle exhaust profiles as a function of nozzle radius. Profiles are supplied for the normal, radial, and tangential nozzle exit velocities, UN, UR, and UT, respectively. Profiles are also supplied for the nozzle exit pressure, temperature, turbulent kinetic energy, dissipation rate of turbulence kinetic energy, and the gas composition, P, T, K, D, and C, respectively. The boundary condition subroutine reads these axisymmetric profiles and interpolates them onto the appropriate boundaries in the 3D grid system. As a note, the actual numbers presented in Table 3-4 are for illustrative purposes only. The tables for actual calculations contain a larger sampling of profile points to adequately capture the gradients at the nozzle exit. This boundary condition subroutine was effectively applied for the steady-state 3D seat demonstration calculation with rocket power on.

Table 3-3. Example Input for Multiple Rockets with Controllable Propulsion

Time	Pin.Pos. #1	Pin.Pos. #2	Pin.Pos. #3	Pin.Pos. #4
0.00	0.15	0.15	0.15	0.15
0.10	0.25	0.25	0.05	0.05
0.20	0.10	0.10	0.10	0.10
0.30	0.05	0.05	0.25	0.25
0.40	0.10	0.10	0.15	0.15
0.50	0.20	0.20	0.25	0.25
0.60	0.10	0.10	0.10	0.10
0.70	0.05	0.05	0.05	0.05
0.80	0.10	0.10	0.10	0.10
0.90	0.05	0.05	0.20	0.20
1.00	0.10	0.10	0.05	0.05

Table 3-4. Example Input for 3D Nozzle Boundary Condition

Description: Pintle Nozzle Position 0.25 in.								
Nozzle Centerline Points: (0.136,0.510,-0.267), (0.283,0.472,-0.196)								
Radius	U	UR	UT	P	T	K	D	C
0.000	1867.	112.	0.0	2.03E6	2236.	12300.	3.85E8	1
0.025	1908.	242.	0.0	1.96E6	2159.	16392.	4.48E8	1
0.050	1945.	268.	0.0	1.88E6	2074.	18954.	5.25E8	1
0.075	1975.	310.	0.0	1.83E6	2016.	22249.	4.45E8	1
0.100	1987.	352.	0.0	1.68E6	2026.	25768.	3.85E8	1
0.125	1935.	438.	0.0	1.74E6	2154.	30852.	7.28E8	1
0.150	1853.	476.	0.0	1.79E6	2179.	36002.	7.76E8	1
0.175	1768.	512.	0.0	1.67E6	2286.	28331.	8.19E8	1
0.200	1623.	329.	0.0	1.62E6	2458.	27459.	9.32E8	1
0.250	0.000	0.00	0.0	1.58E6	2748.	26438.	2.82E9	1

3.4 CFD-ACE Local Grid Refinement Methodology Adaptations

The accurate simulation of the aerodynamic effects of rocket plumes is based upon an accurate prediction of the plume shape and the surface pressures near the plume base. For a CFD analysis, this implies adequate grid resolution for capturing the extreme flow gradients present in rocket plume flowfields. However, this need for high grid resolution must be balanced by the need for a **practical and computationally efficient** engineering tool.

For this project, a multi-domain approach was adapted for accurately and economically predicting the aerodynamic behavior of the complex geometry of the ejection seat and occupant with multiple rockets firing. The major advantage of this multi-domain method is the capability to use many-to-one cell interface meshing. In this method, a coarse grid can be used in one domain while a much finer grid can be used in an adjacent domain. The interface between the two domains involves one cell on one side of the interface, and many cells on the other side of the domain interface. The flow field solution across the interface is solved for in a coupled and fully conservative manner. The obvious advantage of this method is the ability to use fine grids in the immediate

surroundings of the seat and rocket plumes to resolve regions of high flow field gradients, while employing coarser grids in the near-free-stream regions away from the seat and rocket plumes. This methodology allows for an accurate and efficient means of analyzing the effects of rocket plumes on escape system aerodynamics.

As a validation of the newly adapted many-to-one capability, a benchmark calculation was performed to compare results of the single and many-to-one methodologies. The many-to-one method is illustrated in Figure 3-1 for the solution of flow over a blocked region. For demonstration purposes, the blocked region and computational domain have physical dimensions similar to those of a full scale ejection seat calculation. Furthermore, since the solution is for zero side slip, only half of the physical domain is modeled. In Figure 3-1a, the configuration is modeled by a single domain grid with 21,168 grid cells. In Figure 3-1b, the same geometry is modeled using the newly adapted many-to-one capability of CFD-ACE. This grid topology retains the same grid resolution as the single domain topology in the vicinity of the blocked region. However, a 2-to-1 grid interface is used in regions away from the blocked region to reduce the total number of grid cells required for the calculation. The result is a topology composed of six domains and a total of 3,582 grid cells. A six to one increase in the computational efficiency of the simulation.

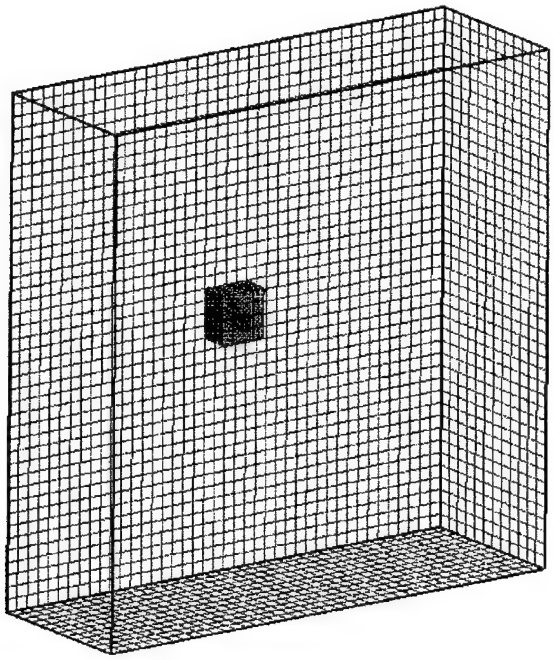

(a) Single Domain Grid

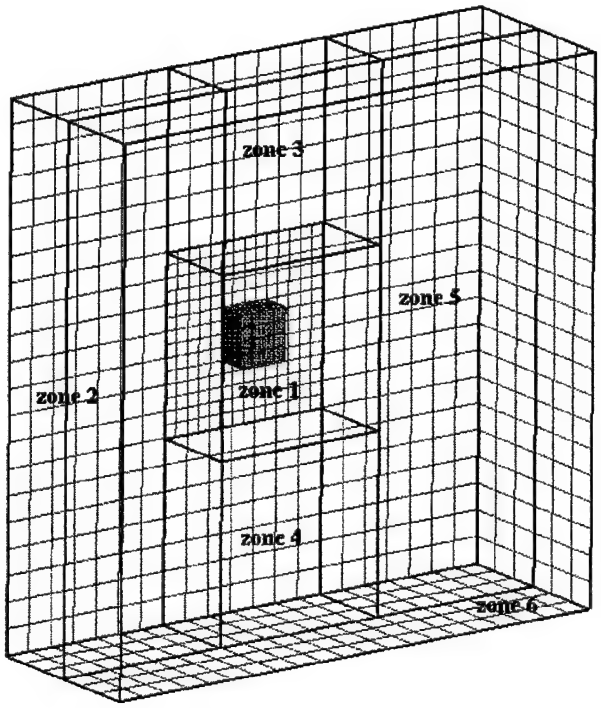

(b) Many-to-One Grid

Figure 3-1. Single and Many-to-One Gridding Methodologies for Flow Over a Block

For applicability, the many-to-one benchmark calculations were performed for the same free-stream conditions as the 3D ejection seat demonstration calculation. These conditions were specifically M_∞ = 0.6, P_∞=4.750e4 Pa, and T_∞ = 290 K. In Figures 3-2 and 3-3, Mach number and Pressure contours for the many-to-one benchmark calculations are presented for the solution symmetry plane. Qualitatively the solutions are very similar in the high gradient region near the blocked surface, the region of primary interest to ejection seat and plume aerodynamic analysis. In the near-free-stream regions surrounding the blocked region a very minor degradation in the solution resolution is observed.

The true test of the many-to-one methodology is its ability to provide accurate and efficient aerodynamic analysis. For ejection system applications, this analysis primarily depends on the prediction of force and moment data. In Figures 3-4 and 3-5, the drag and lift coefficients for the single and many-to-one computations are plotted versus flow solver iteration. (The side force coefficient is omitted due to the symmetry of the computation.) After a brief transient period, the drag and lift coefficients for the two solutions converge to steady-state values. Due to the zero pitch of the configuration, both the single and many-to-one solutions preserve an identically zero lift coefficient, as expected. The effect of the coarser grid of the many-to-one calculation can be seen in the plot of drag coefficient, however. The steady-state drag coefficient predicted by the many-to-one methodology is approximately 2.5% higher than drag coefficient predicted the highly resolved single domain methodology. This 2.5% variation is well with the limits of most engineering problems. Furthermore, this trade off in accuracy resulted in a six-to-one decrease in the time required for flow field solutions. In addition, this 2.5% discrepancy may be avoided if the boundaries of the refined zone are extended outward enough to capture most of the flow gradients.

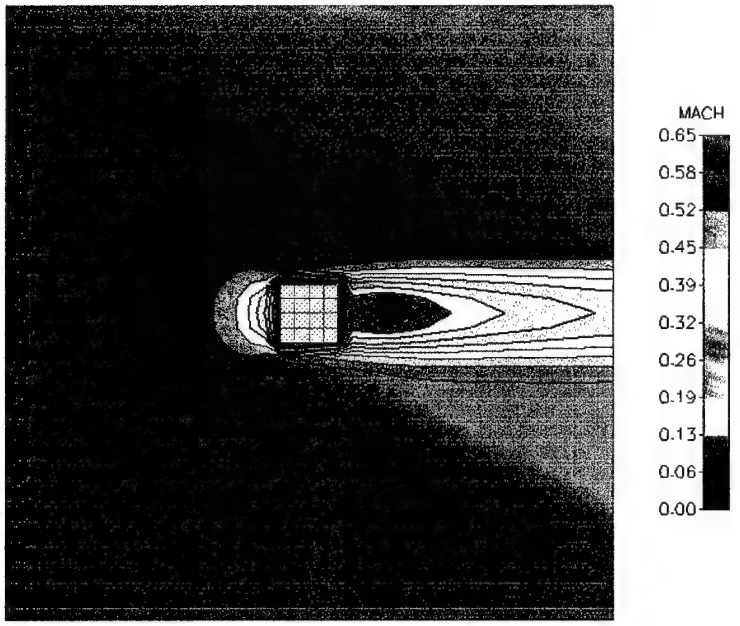

(a) Single Domain Grid

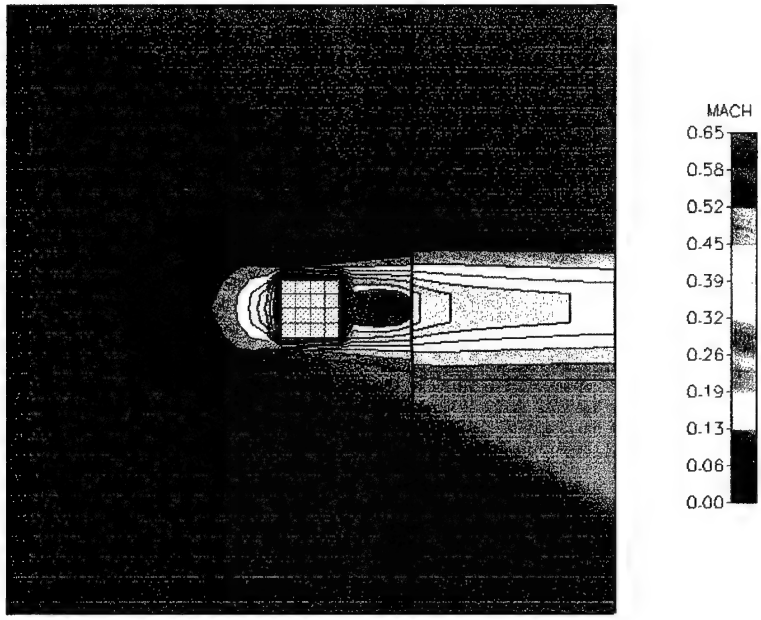

(b) Many-to-One Grid

Figure 3-2. Mach Number Contours for Many-to-One Benchmark Calculation

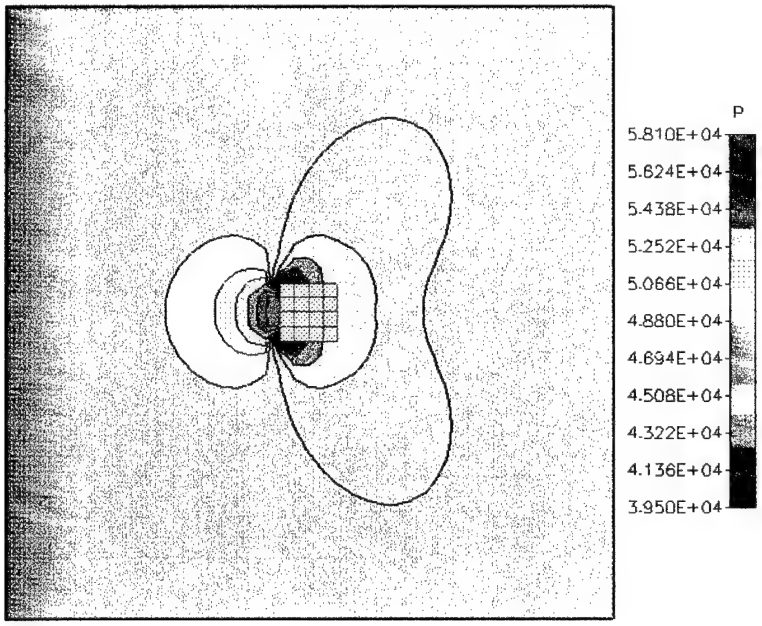

(a) Single Domain Grid

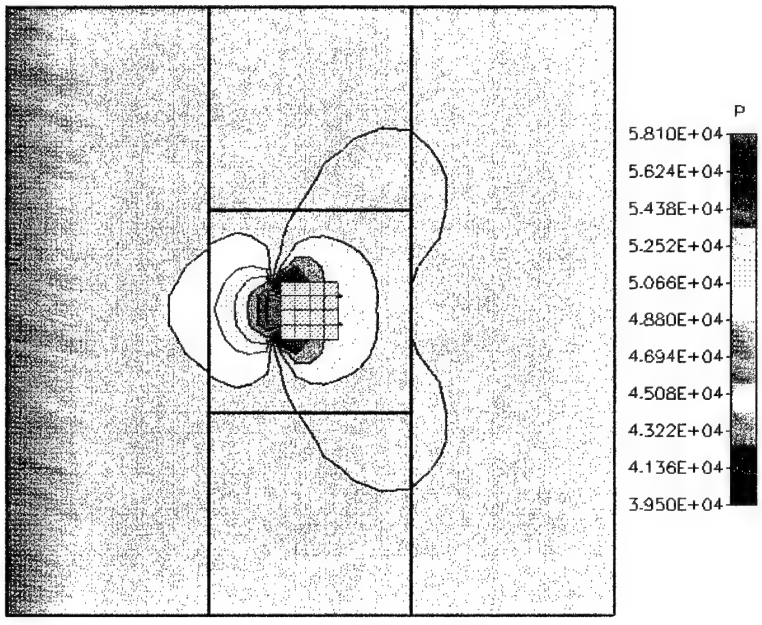

(b) Many-to-One Grid

Figure 3-3. Mach Number Contours for Many-to-One Benchmark Calculation

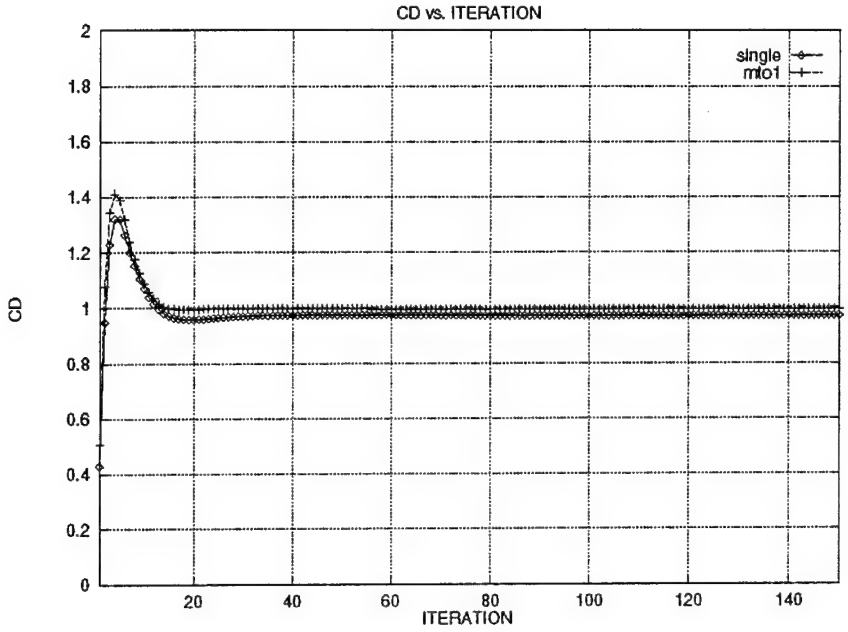

Figure 3-4. Drag Coefficient versus Iteration for Many-to-One Benchmark Calculation

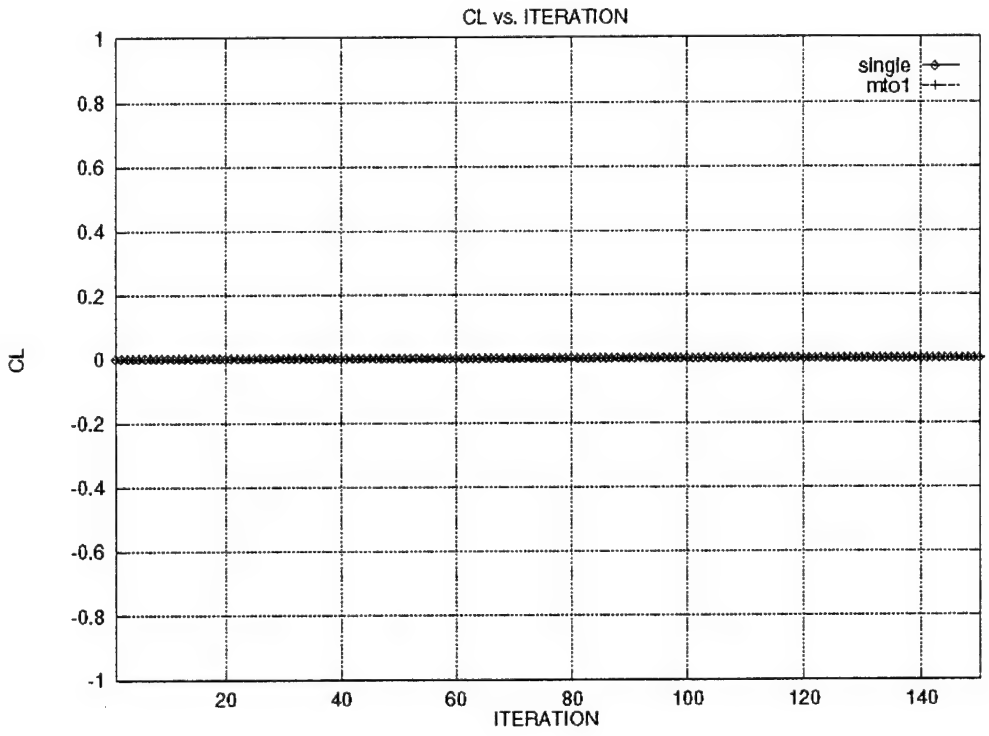

Figure 3-5. Lift Coefficient versus Iteration for Many-to-One Benchmark Calculation

4. INVESTIGATION OF INITIAL AND BOUNDARY CONDITIONS

Various methods for prescribing the rocket plume boundary and operating conditions within the 3D ejection seat computational environment were investigated in this Phase I effort. After initial investigations and problem assessment, it was concluded that, within the 3D environment, solving for nozzle internal flow should be avoided. Instead, a model was developed to prescribe boundary conditions at the nozzle exit. In this project, methods for prescribing nozzle exit conditions were investigated, and grid resolution and spatial differencing studies were performed to assess numerical uncertainties.

To investigate nozzle exhaust boundary conditions and grid resolution issues, a baseline solution for an axisymmetric nozzle and plume was created. Since this task was performed in parallel with the validation efforts of Section 5, the nozzle geometry and flow conditions of the second axial flow validation case were selected (Touron, 1971). The details of the test case are discussed in Section 5.1. In Table 4-1, a matrix of the computations that were performed for the baseline case are presented.

Table 4-1. Computational Cases for Boundary Condition and Grid Resolution Study

Case #	Grid Dimensions	Pjet/Pinf	Composition Plume-F.S.	Nozzle Simulation
1	99x49	5.2	N2-Air	Full Nozzle
2	149x69	5.2	N2-Air	Full Nozzle
3	199x89	5.2	N2-Air	Full Nozzle
4	99x69	5.2	N2-Air	1D Theory
5	99x69	5.2	N2-Air	Profile B.C.

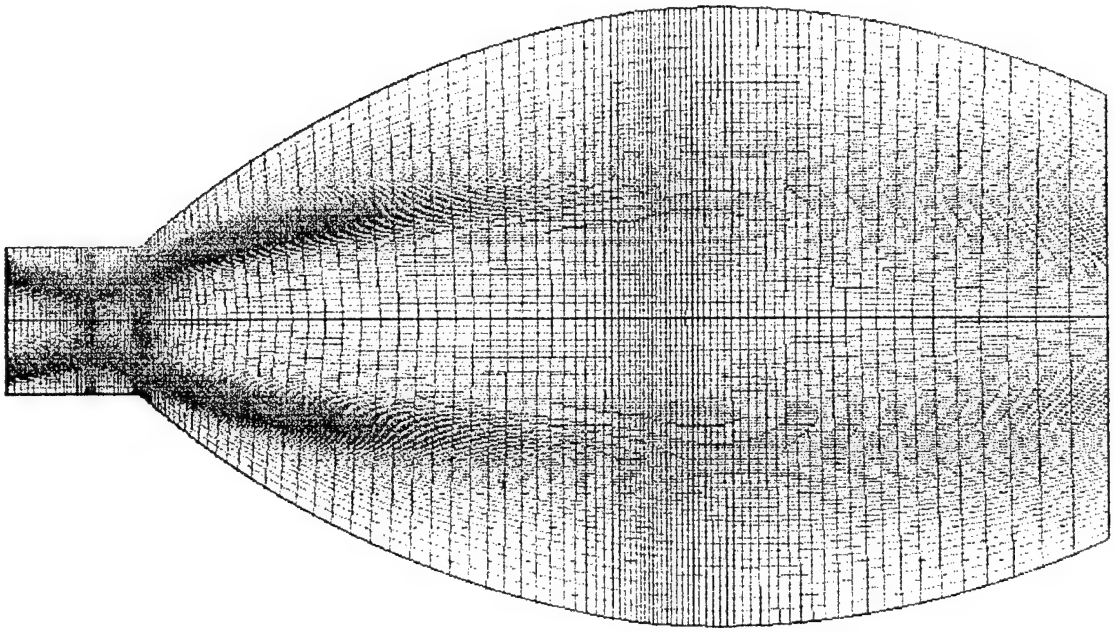

Figure 4-1. Axisymmetric Nozzle and Plume Grid for Case 2, Dimensions 149x69

Cases 1, 2, and 3 were performed for the full nozzle and plume. These three computations were designed to address the issue of grid resolution. The grid for case 2 is shown in Figure 4-1. In Figures 4-2 through 4-4, the computed plume shapes are presented for cases 1, 2, and 3. The solutions were conducted using the k-ε turbulence model with wall functions and first order upwind spatial differencing. The plumes are visualized by plotting the mass fractions of air and N_2. The experimentally observed plume shapes are represented by the symbols overlaid onto the plots. The results show that even the relatively coarse grid of case 1 adequately captured the plume shape. However, some smearing of the plume shape is observed, especially for the coarser grids. To reduce the numerical dissipation of the plume features, an additional computation was performed for grid 2 using a second order upwind spatial differencing scheme. The comparison of the computed Mach contours using both first and second order upwind differencing is presented in Figure 4-5. These results indicate that higher order spatial differencing is equally as important as fine grid resolution for accurately predicting detailed plume features. Therefore, relatively coarse grids can be employed to simulate ejection seat plume flow fields provided that a higher order spatial

differencing is employed, and the grid is approximately aligned with the plume shape. The implications for 3D ejection seat calculations are significant because uniformly fine grids cannot always be employed. However, the task of adequately aligning the grid with the plume structure is more complicated for the 3D ejection seat environment. Therefore, more advanced gridding concepts such as the many-to-one capability were investigated.

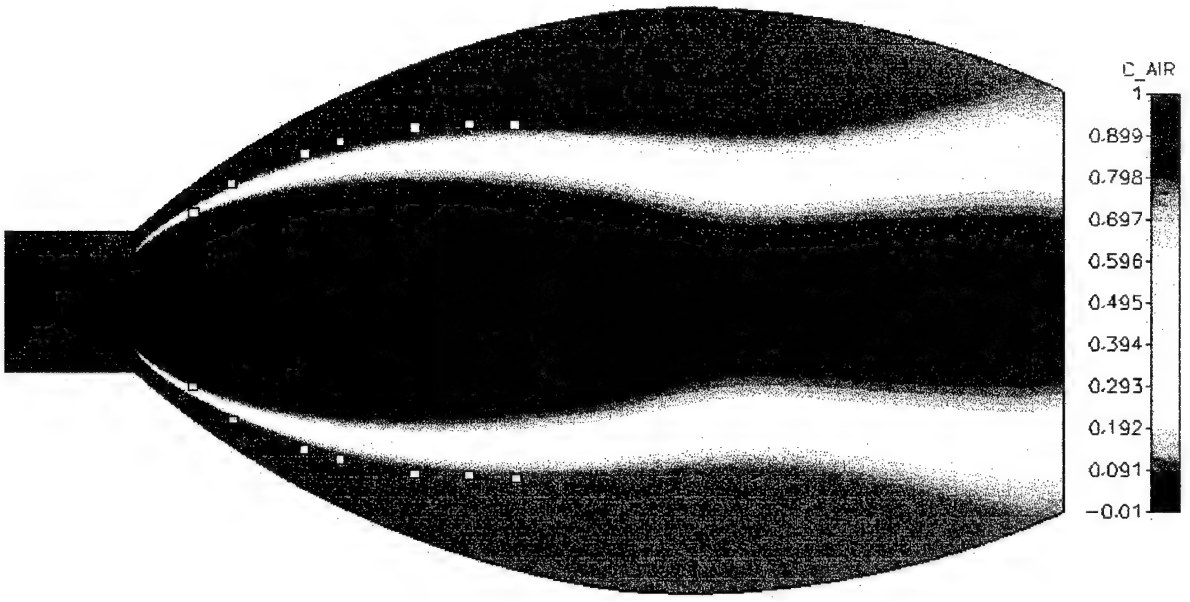

Figure 4-2. Mass Fraction of Air for Validation Case 1, First Order Upwind

With questions of grid resolution and spatial differencing answered, the question of how to replace the full nozzle computation with a nozzle exhaust boundary condition was addressed. For case 4, the axisymmetric nozzle computation was replaced by a constant velocity, pressure, and temperature exhaust boundary condition. The exhaust conditions were calculated using 1D isentropic nozzle theories. The computed plume shape significantly under predicted the measured plume shape. The constant exhaust boundary condition fails because significant variations exist in the actual nozzle exhaust conditions. This fact is demonstrated in Figure 4-6 where the Mach number profile at the nozzle exit is plotted.

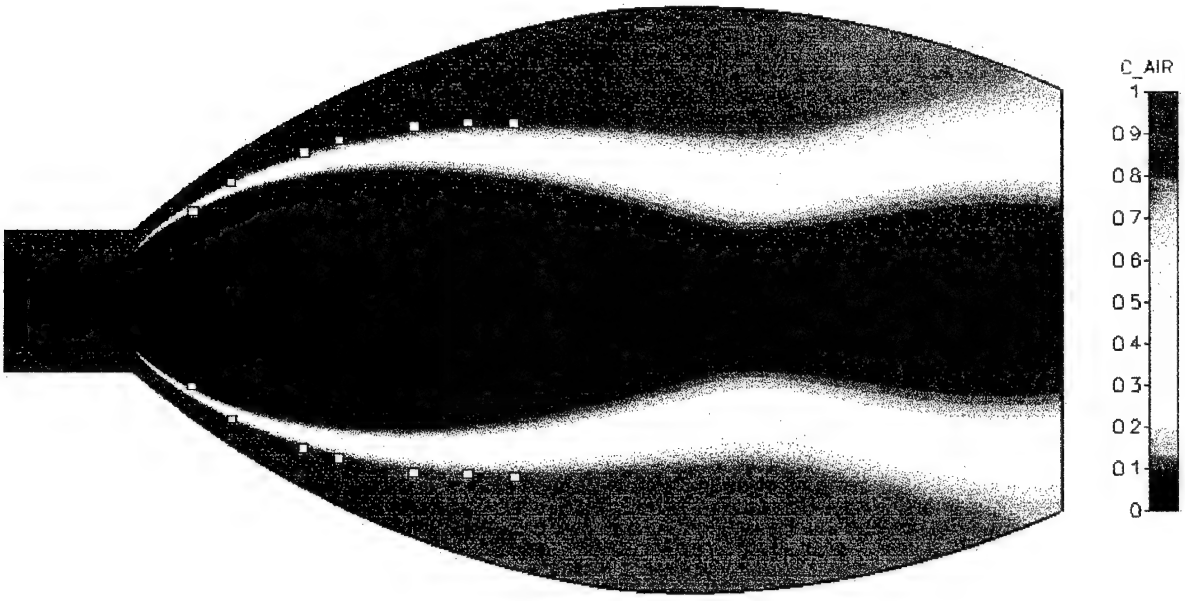

Figure 4-3. Mass Fraction of Air for Validation Case 2, First Order Upwind

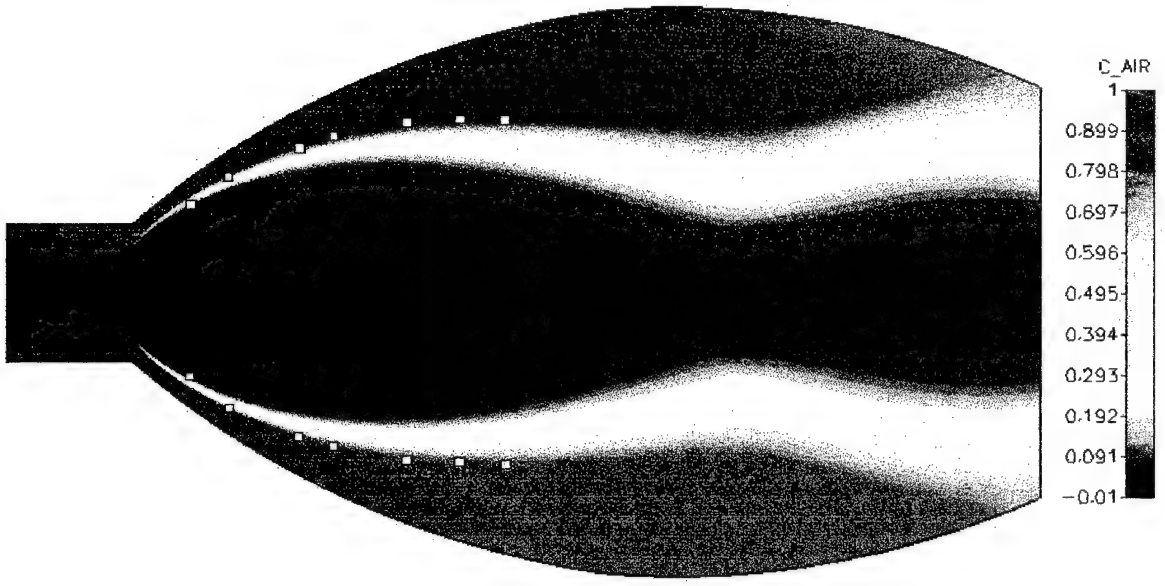

Figure 4-4. Mass Fraction of Air for Validation Case 3, First Order Upwind

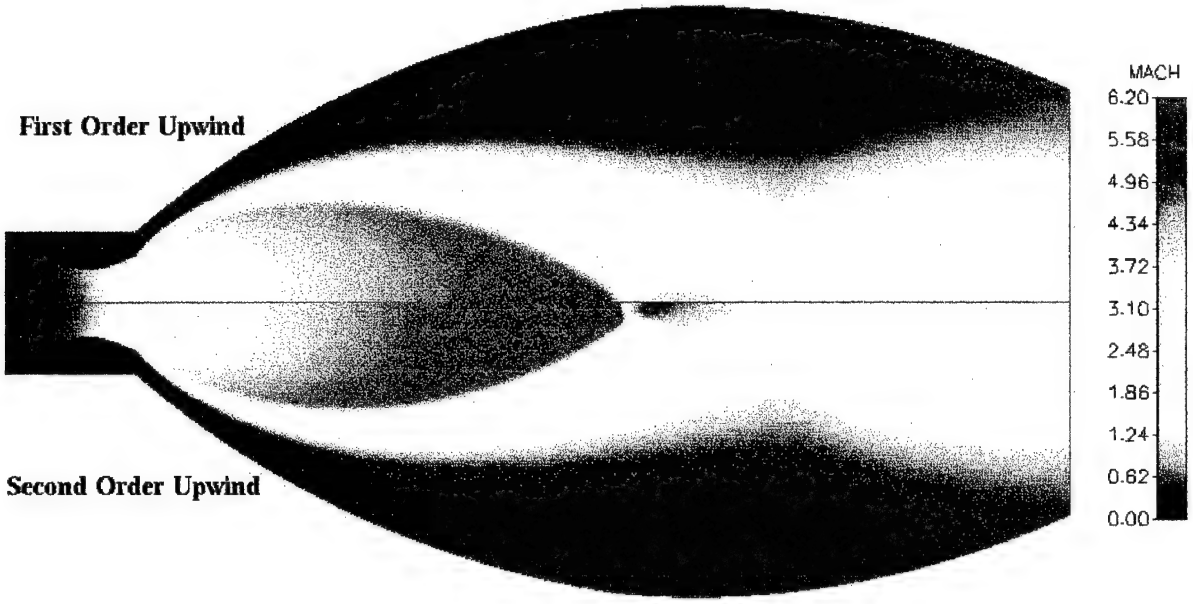

Figure 4-5. Mach Contours for Case 2 using First and Second Order Upwind Schemes

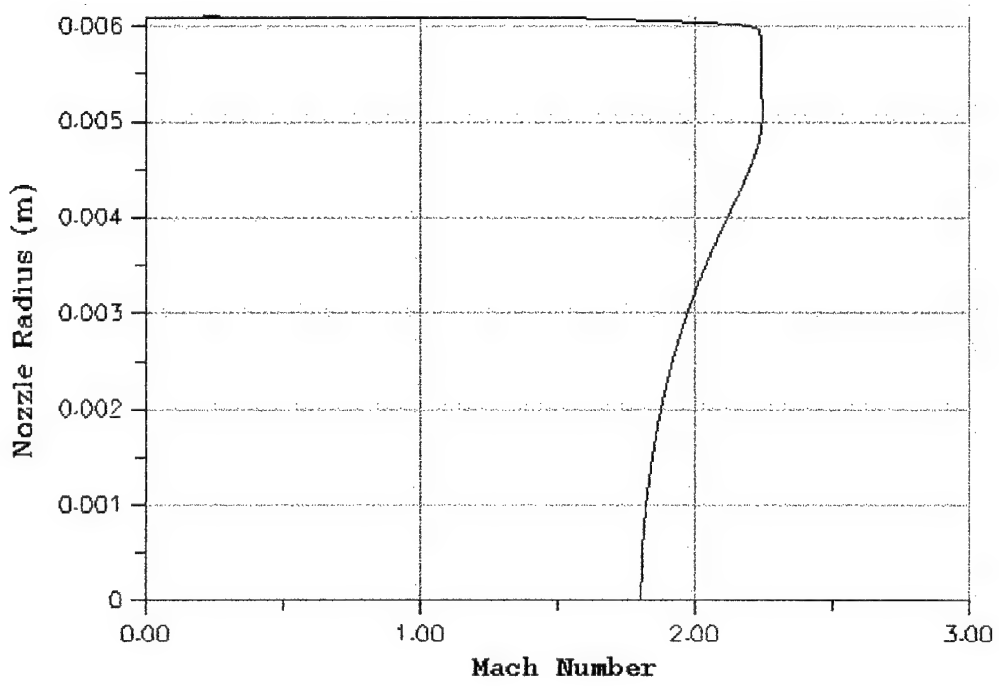

Figure 4-6. Mach Number Profile at Nozzle Exit for Case 2, Second Order Upwind

Based on the non-uniformities that can exist at the nozzle exit, the concept of a constant exhaust boundary condition was abandoned in favor of a profile exhaust boundary condition. As the name implies, the profile boundary condition applies profiles for pressure, velocity, and temperature at the nozzle exit. These profiles are developed by performing an axisymmetric nozzle computation. However, unlike Cases 1, 2, and 3 where the nozzle and plume flow fields are computed simultaneously, the exhaust profile boundary condition allows for the nozzle computations to be performed separately, and the exhaust profiles stored. In Figure 4-7, the computed plume flow field for Case 5 using a profile exhaust boundary condition is compared to the full nozzle and plume flow field computed in Case 2. The computed plume flow fields are nearly identical, thus validating the concept of the profile boundary condition. The profile boundary condition is especially advantageous for the 3D ejection seat environment because it separates the nozzle computations from the 3D ejection seat computations. This separation of the nozzle and plume calculations is important for two reasons. First, 3D nozzle computations performed within the 3D ejection seat environment can drastically effect the convergence and stability of the solutions. In addition, a series of a priori nozzle computations for varying nozzle thrusts can be used to build a look up table of exhaust profiles. This boundary condition table can then be employed in the 3D ejection seat environment to simulate multiple rockets with controllable thrust (See Section 3.3).

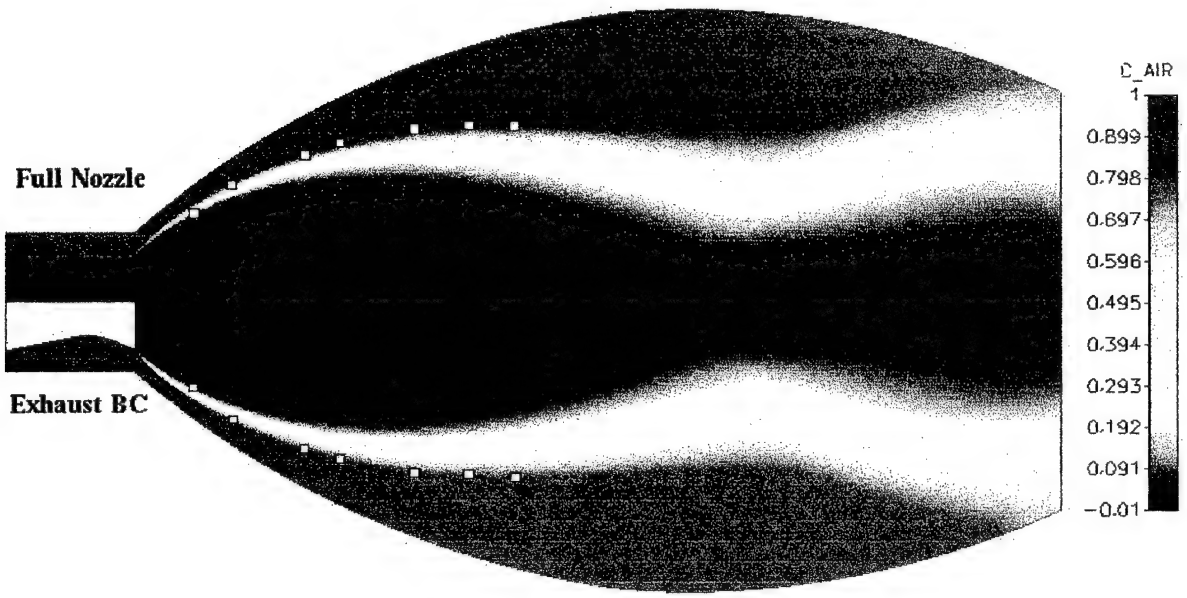

Figure 4-7. Comparison of Computed Plume Shape for Cases 2 and 5

5. BASIC PLUME MODEL VALIDATION

A major objective of Phase I was to validate the basic capability of the developed/ adapted plume model for this project. Two sets of basic validation data were chosen. The first data set was taken from a 0.036 scale B-1A escape capsule (Touron, 1971) test. The data set consists of calibration measurements of model plume shapes for the escape capsule rockets at different jet to free-stream pressure ratios. The second set of experimental data was chosen from the works of Fearn (1978, 1979) and Roth (1989, 1993). This data set consists of measurements of plume velocity centerline and surface pressures for a subsonic jet exiting perpendicularly through a flat plate into a crossflow. This section will describe each test case and present the computational results along with comparison to test data.

5.1 Validation Study for a Plume in an Axial Flow

In 1971 Rockwell conducted a wind tunnel test for a 0.036 scale B-1A escape capsule with simulated rocket power (Touron, 1971). The rocket plumes were simulated using high pressure nitrogen. In designing the rocket nozzles for the wind tunnel model, a series of calibrations tests were performed to ensure that the scaled nozzles accurately reproduced the plume characteristics of the full scale capsule. These calibration tests consisted of measurements of the plume shape for the model main nozzle exhausting into a quiescent back pressure. The calibration conditions reproduced the flight conditions for Mach 0.30 and 0.95 at sea level, and Mach 1.20 at 25,000 feet. The conditions for the simulation are presented in Table 5-1.

Table 5-1. Summary of Axial Flow Nozzle and Plume Validation Cases

Case #	Alt. (ft)	Mjet	Jet - F.S.	Pjet/Pinf	Ajet/A*
1	Sea Level	2.35	N2-Air	4.9	2
2	Sea Level	2.35	N2-Air	5.2	2
3	25000	2.35	N2-Air	11.1	2

Axisymmetric turbulent and compressible computations were performed with CFD-ACE for all three conditions. The simulations modeled the complete mixing problem of the nitrogen plume with a quiescent air back pressure. The k-ε turbulence model was used in computations, as well as, second order upwind spatial differencing scheme. The

computations were performed on the 99x69 axisymmetric grid shown in Figure 5-1.

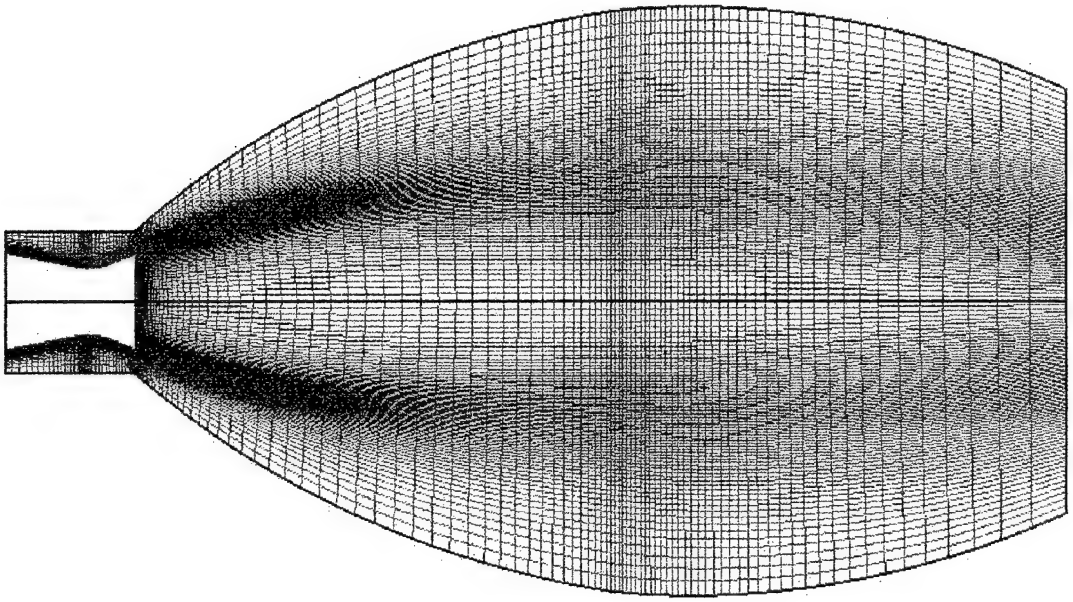

Figure 5-1. Nozzle Geometry and Grid for 0.036 Scale B1 Escape Capsule

The nozzle exhaust boundary conditions were applied using the profile method discussed in Section 4. Figures 5-2 through 5-4 show the computed plume flow fields. The plume shape is visualized by plotting both the mass fraction of air and the Mach number. The symbols represent measured plume shapes from the calibration tests. Excellent agreement between the predicted and measured plume shapes is seen for all three test conditions. Note that regardless of the different shape and size of the plume, and eventhough the same grid was used for all three calculations, very good agreement was obtained. This demonstrates that local grid adaptation is not necessarily needed to capture the overall shape of the plume. What is important, however, and as seen in the previous section is at least a second order differencing scheme and a reasonable grid resolution are needed for proper rocket plume simulations.

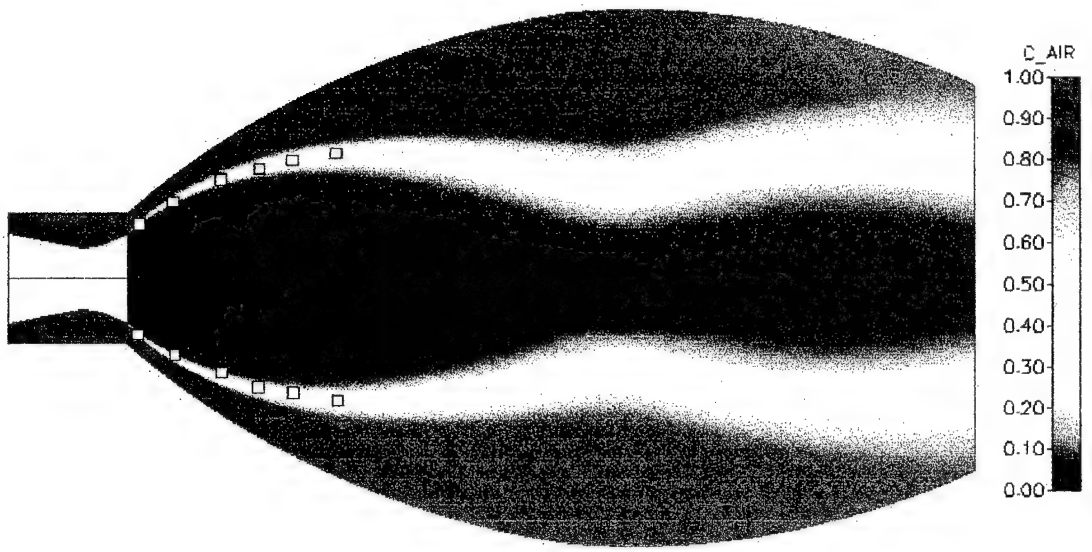

(a) Mass Fraction Contours for Air

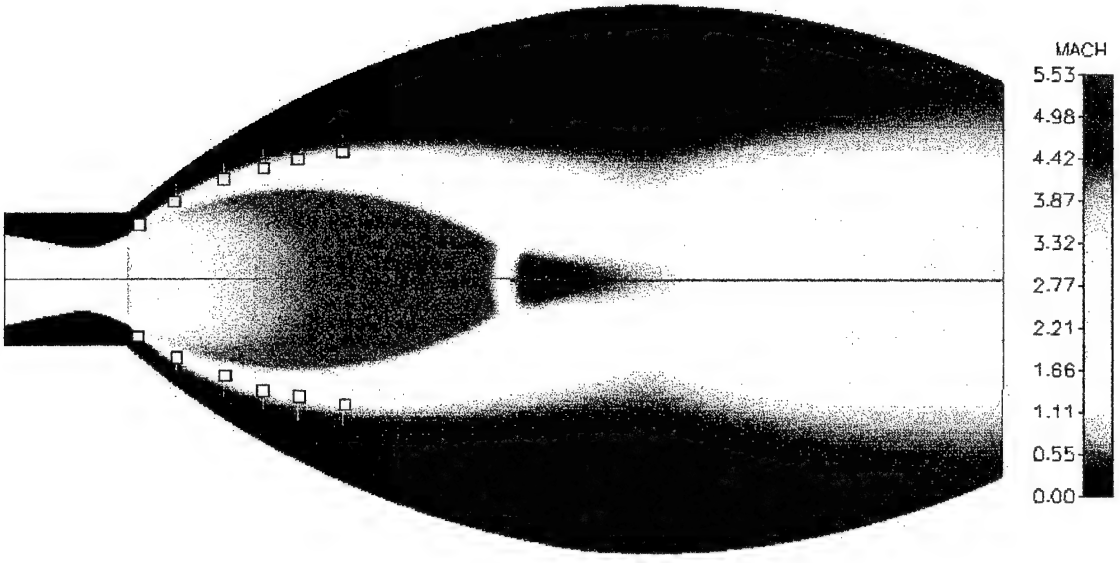

(b) Mach Number Contours

Figure 5-2. Predicted Plume Shape for Validation Case 1

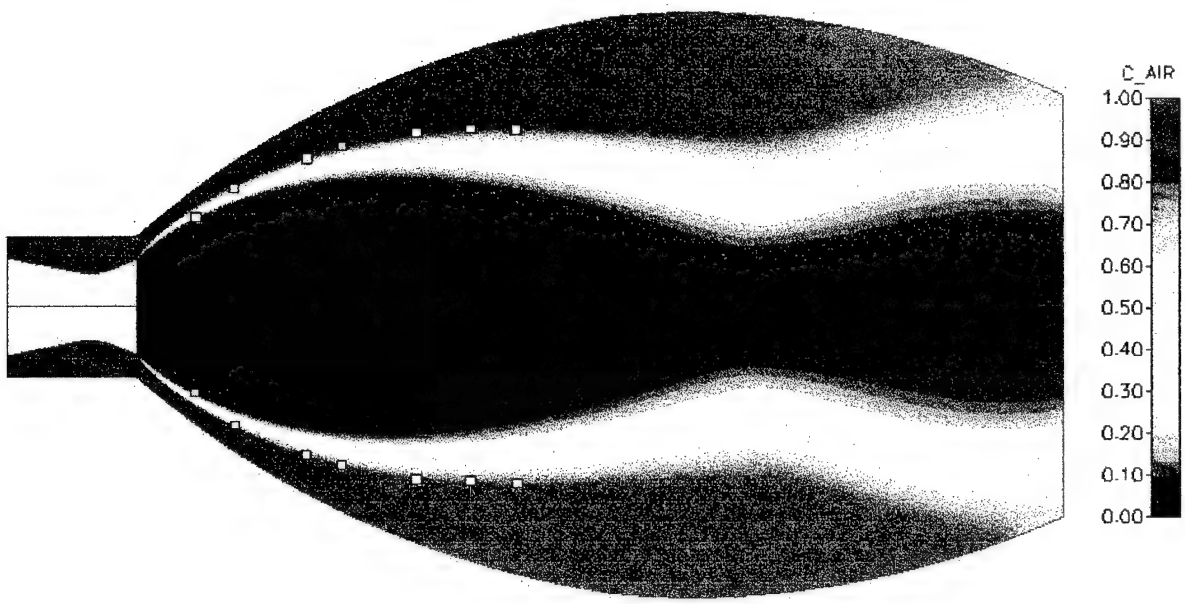

(a) Mass Fraction Contours for Air

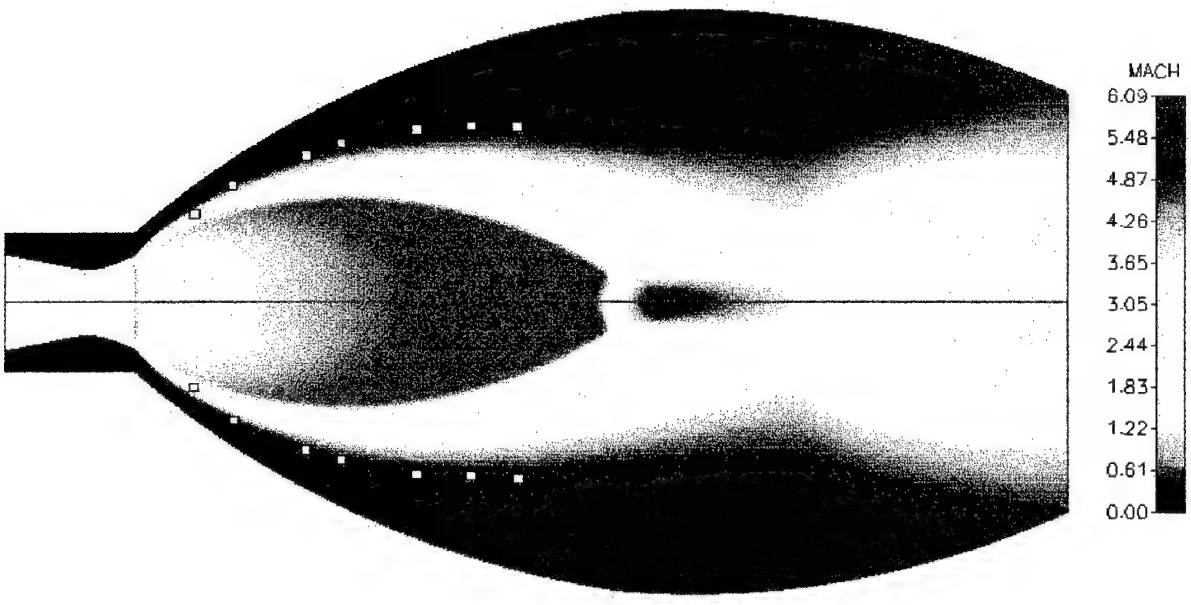

(b) Mach Number Contours

Figure 5-3. Predicted Plume Shape for Validation Case 2

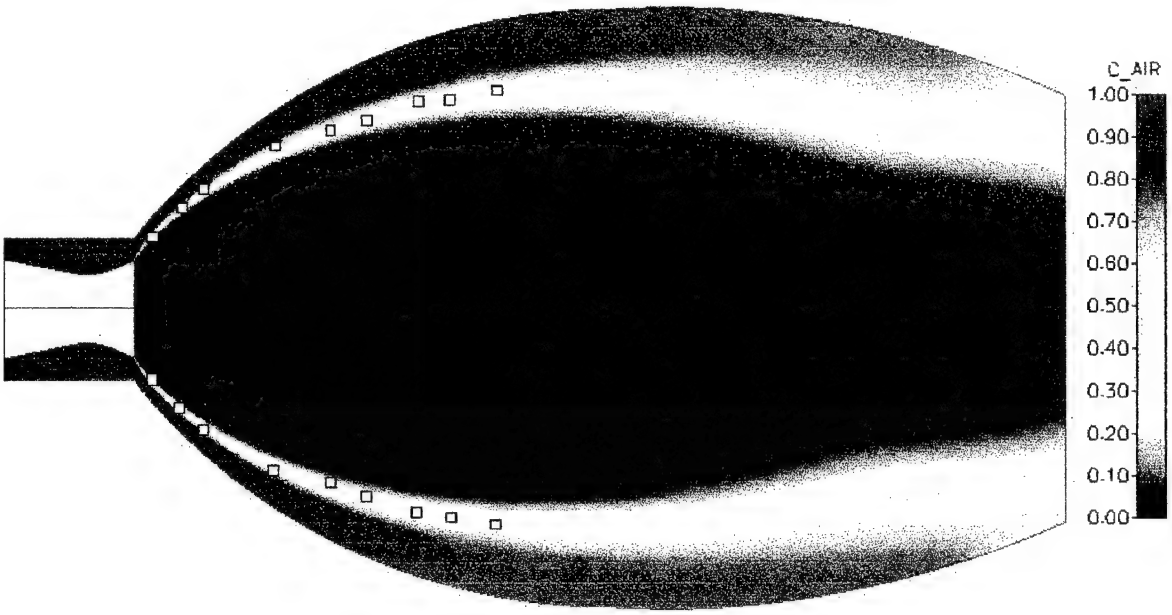

(a) Mass Fraction Contours for Air

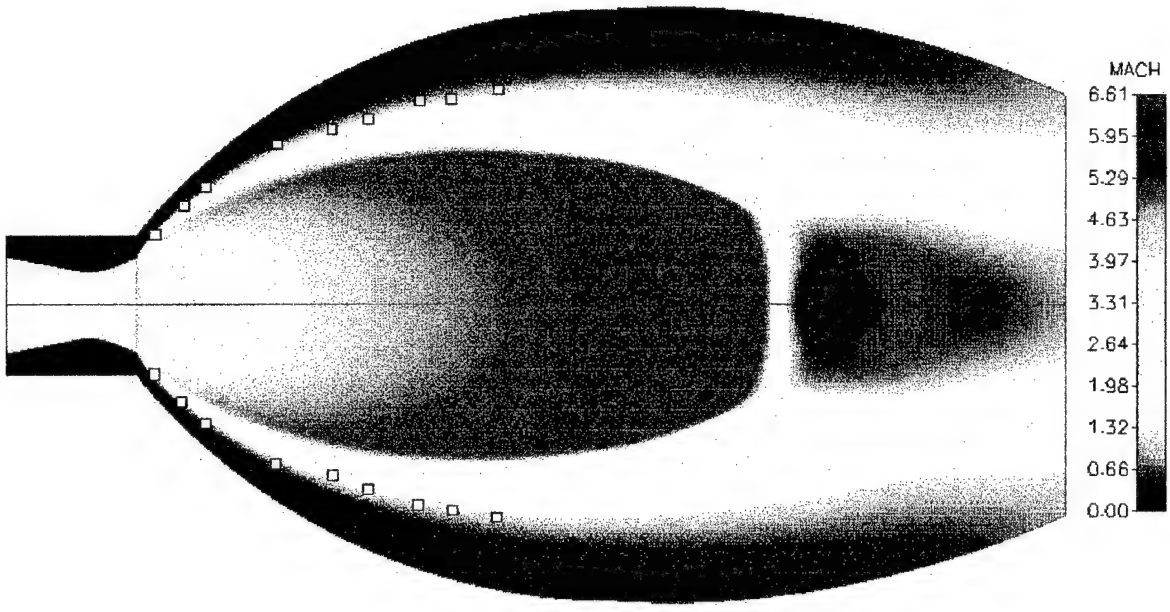

(b) Mach Number Contours

Figure 5-4. Predicted Plume Shape for Validation Case 3

5.2 Validation Study for a Plume in a Crossflow

Fearn and Weston (1979, 1989) conducted a series of tests at NASA Langley to investigate the flow field associated with a jet in a crossflow. The experimental apparatus consisted of a 4 ft. by 9 ft. flat plate mounted above the tunnel floor with a 4 in. diameter jet orifice exiting perpendicular to the free stream flow 3 ft. downstream of the leading edge of the plate. The plate was instrumented to measure plate pressures upstream of the jet (0 deg.), downstream of the jet (180 deg.), and laterally to the jet (90 deg.), see Figure 5-5. Velocity measurements were also taken in the jet to determine the velocity centerline. This velocity centerline is defined as the locus of the maximum velocity in the direction of the jet.

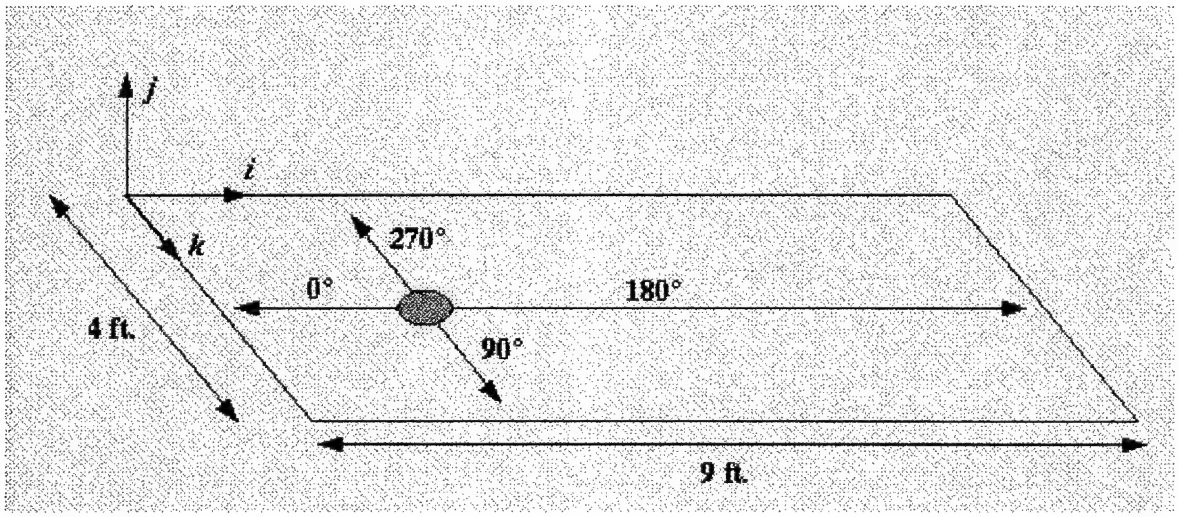

Figure 5-5. Schematic of Experiment for Jet in a Crossflow

The determining characteristic for a jet in a crossflow is the ratio of the jet to free stream momentum. When the density of the jet and free stream are the same, and the velocity of the jet is constant over the jet orifice (as is the case here), then the determining characteristic reduces to the ratio of the jet and free stream Mach numbers, $R = Mj/M\infty$. The simulated conditions for the test case studied here is R=4, $M\infty = 0.2$, and Re = 500,000. For this test case the jet and free stream pressure and temperature were also equal.

The above case was simulated with CFD-ACE using a 55x55x50 Cartesian grid. The computation utilized a symmetry plane through the axis of the jet. The k-ε turbulence model with wall functions was employed with a y+ at the wall of approximately 50. The solutions were performed using the second order accurate central differencing scheme. In Figure 5-6, the velocity vectors in the symmetry plane and just above the flat plate are presented. The velocity vectors are also colored by Mach number. In addition to the velocity vectors, blue colored stream traces were released upstream of the jet and red stream traces were released inside the jet to visualize the global features of the flow. Entrainment of the upstream stream traces by the jet is observed. This entrainment is caused by a pair of contrarotating vortices that develop near the exit of the jet orifice. These contrarotating vortices are caused by the distortion of the shear layer. Also evidenced are the horseshoe vortices that develop in the boundary layer of the plate.

In Figure 5-7, the jet velocity centerline is compared to the experimental profile. The computed plume shape is in excellent agreement with the measurements up to x/D of about 6. Further downstream, the shown discrepancy may be due to reduced grid resolution that in turn results in more dissipation of upstream information. Refining the grid in these areas has to be done in light of its effects on surface pressures and economic factors. In Figure 5-8, the surface pressures are compared to experiment. Comparisons of pressure coefficient for the 0 deg. and the 90 deg. rays are very good. Note that the test data were scanned from a published paper, and there may be some errors involved in experimental data representation. In the wake of the plume (180 deg.), the discrepancy between the measured and computed pressures is larger. The accurate prediction of the pressures in the wake of the plume is strongly influenced by the turbulence model employed. Roth (1989) and Chiu (1993) report similar difficulties in matching the pressure distribution in the wake of the jet. Chiu (1993) attributes these difficulties to current limitations in turbulence modeling. This issue will be further investigated in phase II of this study as alternative versions of K-ε turbulence model as well as other turbulence models will be explored and tested on this problem.

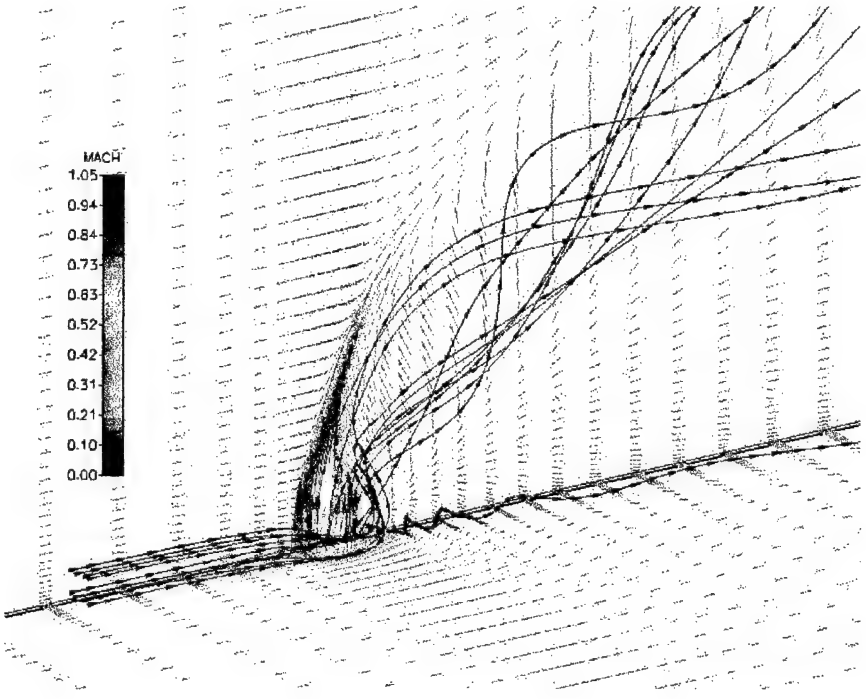

Figure 5-6. Velocity Vectors in Symmetry Plane for R = 4

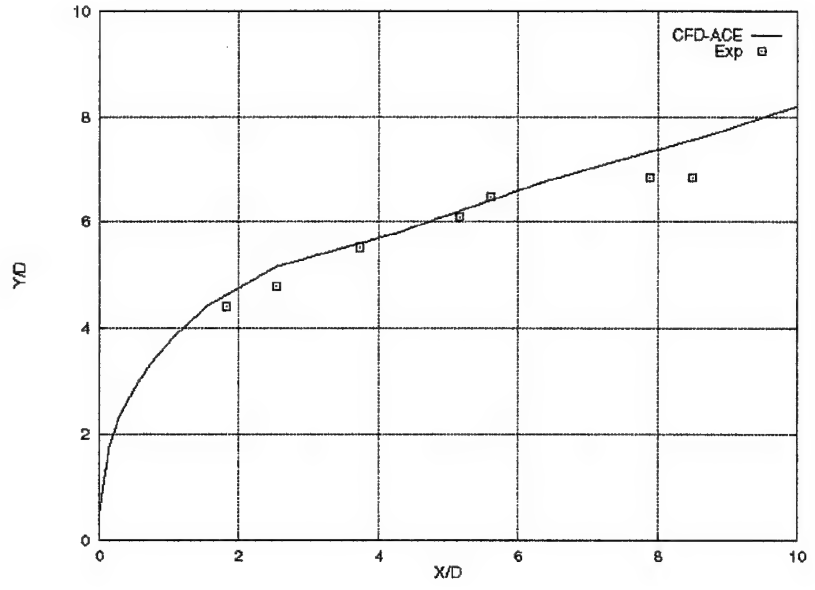

Figure 5-7. Computed and Experimental Jet Centerline for R = 4

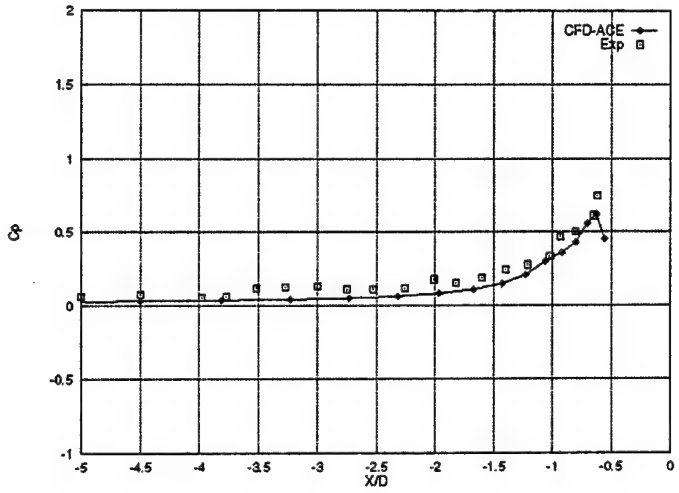

(a) θ = 0 deg

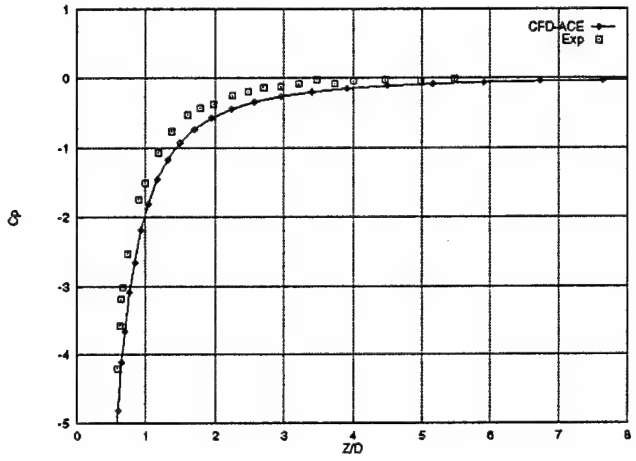

(b) θ = 90 deg

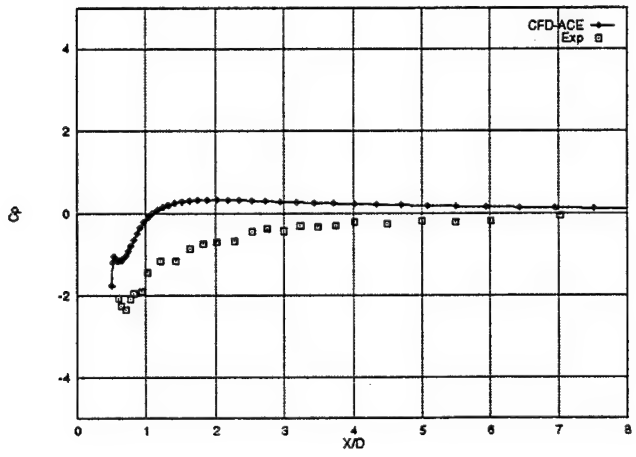

(c) θ = 180 deg

Figure 5-8. Plate Pressure Distribution Along Rays

6. DEMONSTRATION AND VALIDATION FOR PEPS

6.1 Discussion of PEPS Nozzle Testing by Aerojet Corporation

The basis of this validation study was a preliminary test program conducted by Aerojet Corporation in 1994 (McDonnell Douglas, 1995). The third phase of this program was a static ground test of the PEPS motor in the full "H" configuration with four actuated pintles, see Figure 6-1. The test operated the pintle nozzles at a chamber pressure of 2500 psi in a duty cycle that commanded the motor to perform a pitch, a yaw, and then a pitch maneuver. These pitch and yaw maneuvers were performed by independently controlling the pintle position, and thus the thrust, of each of the four rocket nozzles. Detailed time histories of the thrust and pintle positions for each nozzle were recorded. The time histories for thruster 1 are shown in Figure 6-2. The time histories for the other three thrusters are similar. In Figure 6-2a, the commanded and actual pintle positions are shown. Figure 6-2b contains the actual thrust and the thrust predicted by the Aerojet Transient Analysis 1-D code (ATA1D) (McDonnell Douglas, 1995). By comparing the actual thrust and actual pintle position histories, a correlation between pintle position and nozzle thrust was developed. These correlations formed a basis for validating the updated capabilities of CFD-ACE and will be discussed in detail in Section 6.3.

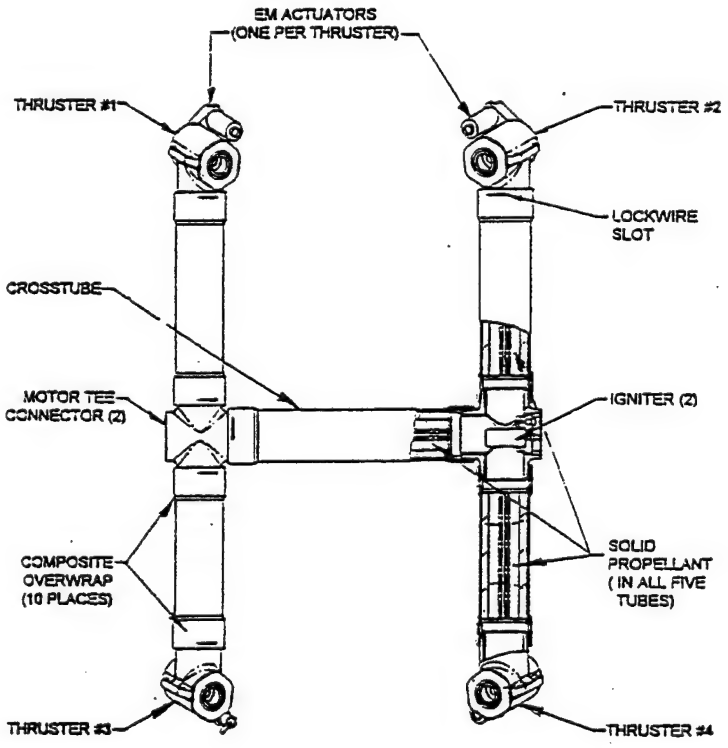

Figure 6-1. Aerojet's Pintle Escape Propulsion System (PEPS) (McDonnell Douglas, 1994)

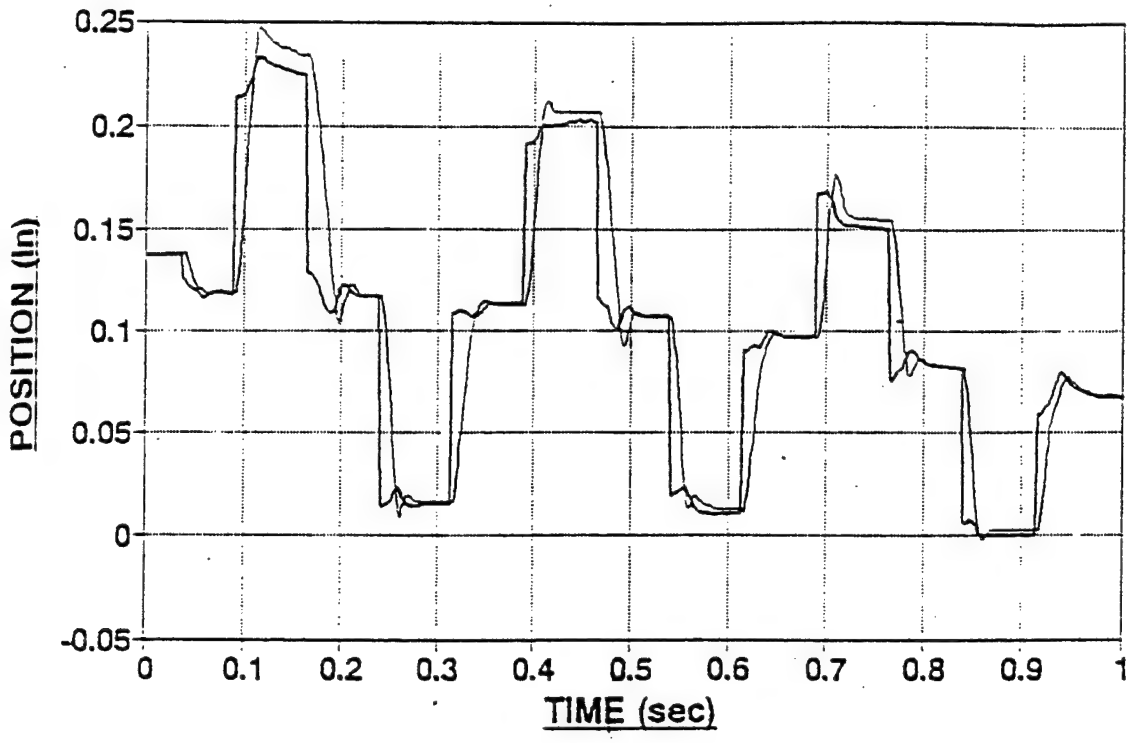

(a) Commanded and Actual Pintle Position vs Time

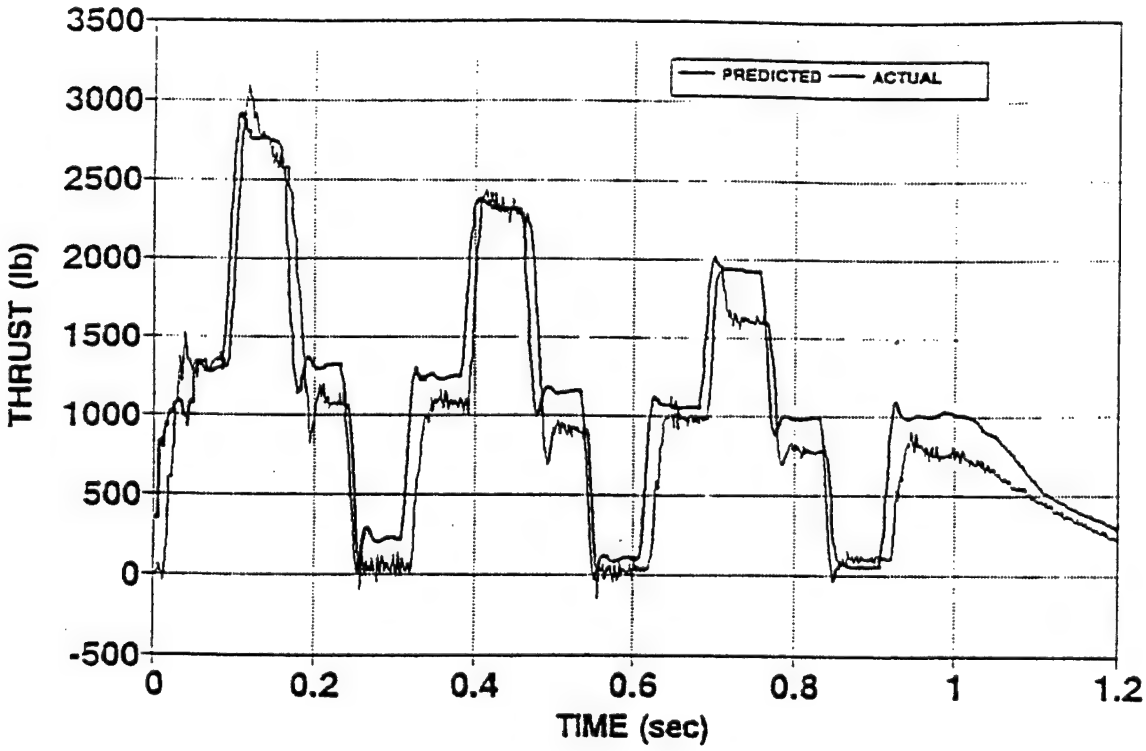

(b) ATA1D Predicted and Actual Thrust vs Time

Figure 6-2. Aerojet Initial Test 3, Thruster 1 Performance (McDonnell Douglas, 1994)

6.2 Discussion of PEPS Nozzle Analysis by CFDRC

A series of axisymmetric, frozen and equilibrium solutions was performed for a single PEPS rocket nozzle for comparison to the above test program, see Table 6-1. For these computations the pintle position was varied from 0.05 in. to 0.25 in. from the nozzle throat. (For convenience, the pintle position was defined as the distance between the nozzle throat and the tip of the pintle.) An additional computation was also performed for the nozzle without the pintle to assess the maximum nozzle thrust. To assess the importance of chemistry effects, both equilibrium and frozen chemistry solutions were performed for the 0.25 in. pintle position. This series of calculations served as a validation of the updated chemistry capabilities of CFD-ACE, as well as, provided realistic nozzle exhaust boundary conditions for the 4th Generation Ejection Seat demonstration calculation (see Section 6.5).

The pintle and nozzle geometry for the PEPS motor was created using CFD-GEOM and design drawings provided by Aerojet Corporation. Figure 6-3 contains a 3D rendering of the pintle geometry. The pintle was initially located such that the pintle tip was 0.25 in. from the nozzle throat. The resulting geometry was modeled using a two domain, axisymmetric grid with dimensions 26x26 and 51x51, respectively. A viscous wall spacing of 1.0E-04 m was applied. The computational domain extended from the nozzle inlet to the nozzle exit. The computational grids for the other pintle positions were easily created in CFD-GEOM by translating the pintle geometry with respect to the nozzle geometry. CFD-GEOM automatically updates the computational grids whenever the associated geometries are altered. The computational grids for all six pintle positions are shown in Figure 6-4.

Table 6-1. Computational Cases for Pintle Nozzle Flowfield Study

Case #	Pintle Pos. (in)	Spatial Diff.	Chemistry
1	0.25	2nd Order Upwind	Equilibrium
2	0.25	2nd Order Upwind	Frozen
3	0.20	2nd Order Upwind	Frozen
4	0.15	2nd Order Upwind	Frozen
5	0.10	2nd Order Upwind	Frozen
6	0.05	2nd Order Upwind	Frozen
7	none	2nd Order Upwind	Frozen

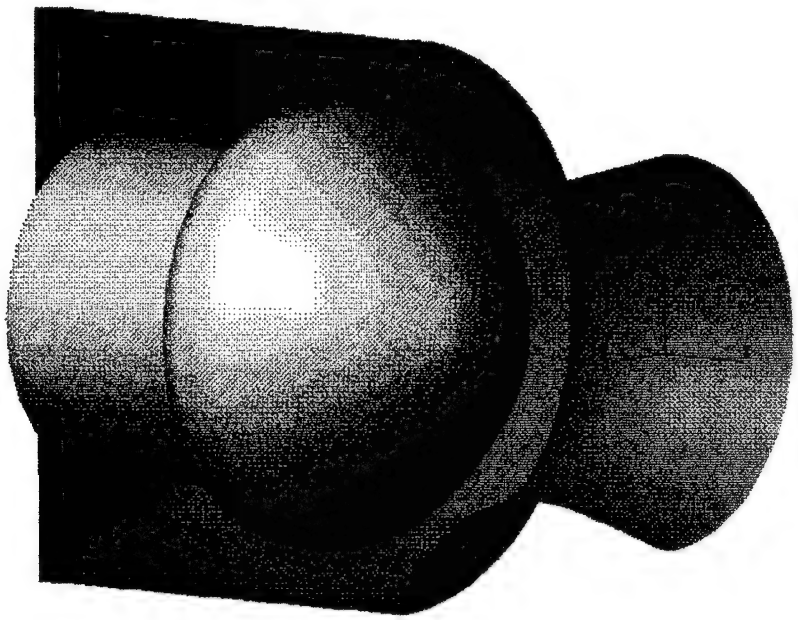

Figure 6-3. Axisymmetric Pintle Nozzle Geometry Created Using CFD-GEOM

All of the computational cases were conducted using the second-order upwind spatial differencing scheme and the k-ε turbulence model. The gas properties were specified using the updated chemistry database discussed in Section 3.2. The boundaries of the computational domain were specified in the following manner. A total pressure and total temperature boundary condition was applied at the nozzle inlet with P_T = 2500 psi (1.724E7 Pa) and T_T = 4981 F (3023 K). The chemical composition at the nozzle inlet was specified according to Table 3-2, Section 3.2. An extrapolation boundary condition was applied at the nozzle exit where the flowfield was supersonic. The pintle and nozzle walls were modeled with a viscous, adiabatic wall condition, and a symmetry condition was applied along the centerline of the nozzle.

The thrust and mass flow for each case were computed by numerically integrating the following equations at the nozzle exit:

$$\dot{m} = 2\pi \int_0^R \left[\left(\rho u_x^2 + \left(P_e - P_\infty \right) \right) \right] r \, dr$$

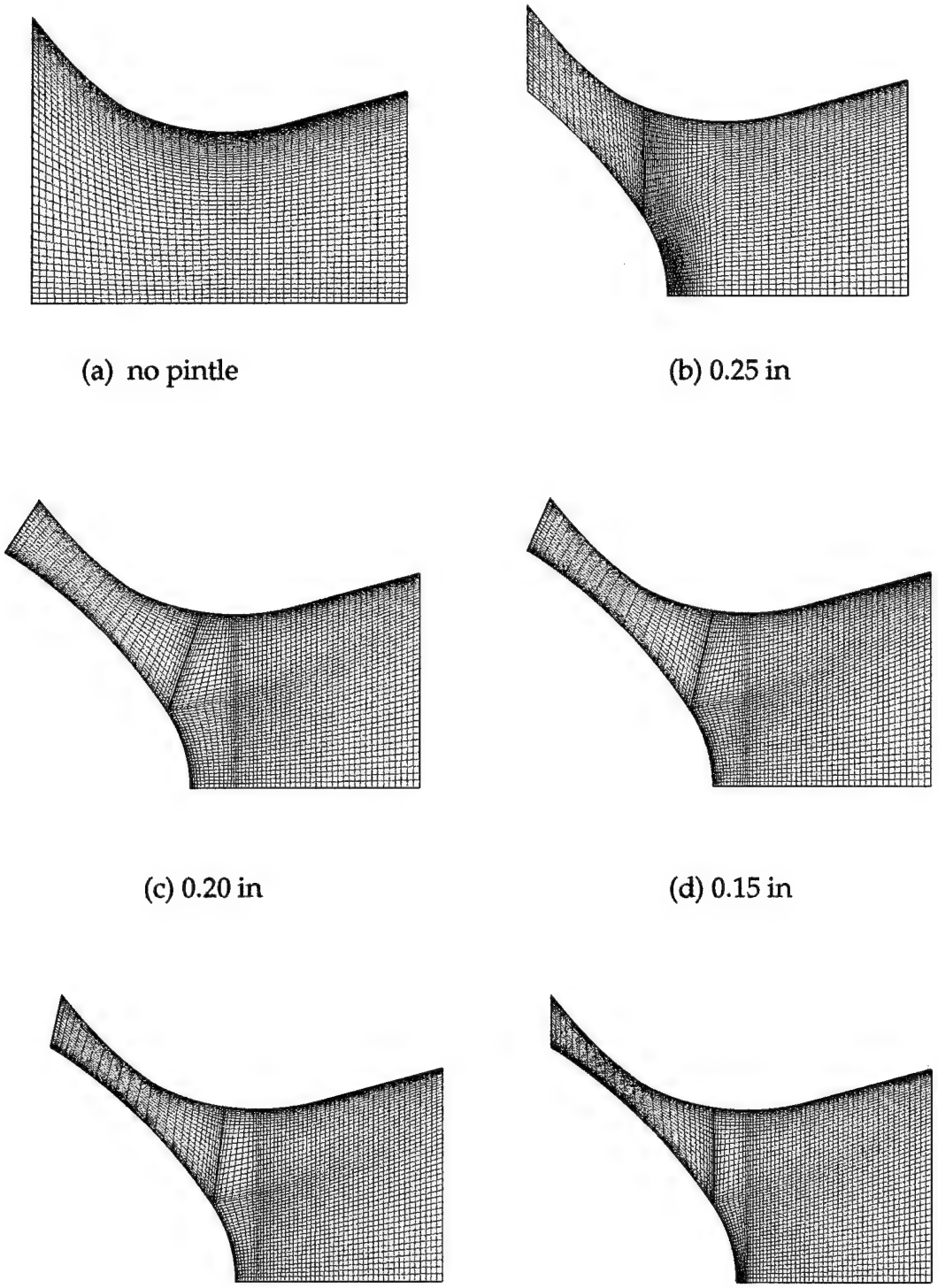

(a) no pintle

(b) 0.25 in

(c) 0.20 in

(d) 0.15 in

(e) 0.10 in

(f) 0.05 in

Figure 6-4. Axisymmetric Pintle Nozzle Grids, Dimensions: 26x26 and 51x51

$$T_x = 2\pi \int_0^R [\rho u]\, r\, dr$$

where r is the radial coordinate, R is the nozzle exit radius, and P_∞ = 1 atm.

The equilibrium chemistry and frozen chemistry solutions for the 0.25 in. pintle position, cases 1 and 2, were performed first to assess the effects of the rocket chemistry on the gross flow field properties. (Details of the pintle nozzle flowfield unrelated to the chemistry models will be discussed later.) The equilibrium and frozen solutions represent the limits of the chemical system. The equilibrium solution assumes that the chemical reactions occur infinitely fast, such that the chemical composition is always in local equilibrium. The frozen chemistry solution assumes that the chemical reactions occur infinitely slow, such that the chemical composition does not change. (Note, in the frozen chemistry model, only the gas composition is frozen. The gas properties are still a function of temperature and are calculated according to the database curve fits.) The correct physical solution lies somewhere in between the equilibrium and frozen solutions. A comparison of the equilibrium and frozen chemistry solutions is presented in Figure 6-5. The Mach number and pressure contours for the two solutions are nearly identical. This similarity exists because of the very small differences in the chemical composition of the two solutions. The computed mass flow and thrust for the frozen and equilibrium solutions are 8.93 kg/sec and 1.891 kN versus and 8.87 kg/sec and 1.892 kN, respectively, a difference of less than one percent. Based on this strong correlation between the two solutions, the frozen chemistry model was determined to be sufficient for simulating flow field features of interest. Furthermore, based on the one dimensional calculations presented in Table 3-2, the influence of varying chemical composition in the external plume flowfields is also expected to be negligible. As a result, the remainder of the solutions in Table 6-1 were computed using the frozen chemistry model.

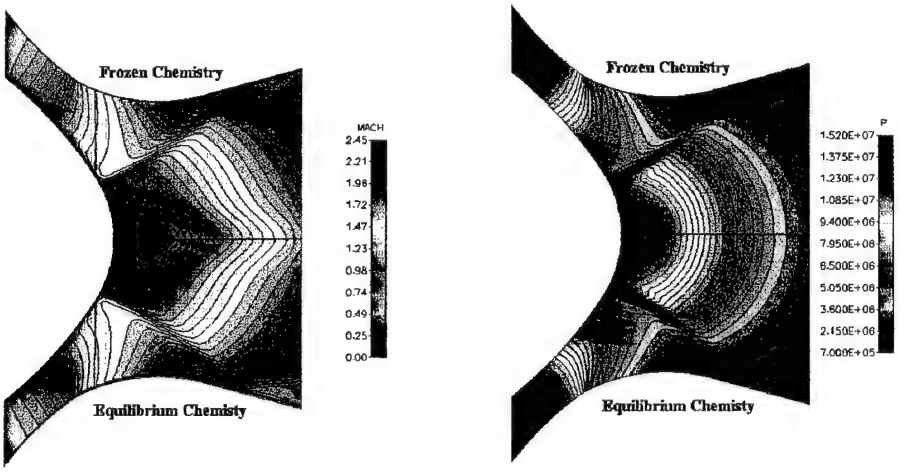

(a) Mach Number (b) Static Pressure

Figure 6-5. Comparisons of Equilibrium and Frozen Chemistry Solutions

The Mach number and pressure contour plots for all six pintle positions computed using the frozen chemistry model, cases 2-7, are presented in Figures 6-6 and 6-7. The thrust and mass flow results are presented in Table 6-2. By examining the series of contour plots and the thrust data, a more thorough understanding of the pintle nozzle operation is obtained.

Table 6-2. Thrust and Mass Flow Rate for Pintle Nozzle Flowfield Study

Pintle Pos.	Mass Flow		Thrust	
inches	kg/sec	lbm/sec	kN	lbf
none	12.8	28.2	26.45	5947.
0.25	8.93	19.7	18.91	4250.
0.20	7.83	17.3	16.57	3725.
0.15	6.65	14.7	14.01	3149.
0.10	5.48	12.1	11.81	2656.
0.05	4.26	9.40	9.42	2117.

Beginning with the baseline nozzle computation (no pintle), the results are similar to the traditional rocket nozzle analysis of Section 5.1. The major difference being that the gas is composed of hot combustion products with a ratio of specific heats of approximately 1.22 and a molecular weight of 26.0 kg/kg-mole. Employing these gas properties and a nozzle area ratio of 1.54, one-dimensional, isentropic nozzle theory predicts constant exit properties of: Mach=1.81, P=3.14E6 Pa, $\dot{m}$=13.1 kg/sec, and T_x=27.28 kN. The axisymmetric results, while not constant, are still in good agreement with the simplified nozzle theory. The predicted thrust and mass flow rates differ by less than 3 percent.

By examining the solutions for the range of pintle positions from 0.25 in. to 0.05 in. the effect of the pintle on the baseline nozzle flowfield is understood. The pintle effects the thrust of the nozzle by altering the effective area ratio of the nozzle. As the pintle moves forward the effective area of the throat is reduced, and thus the mass flow and thrust of the nozzle are reduced. At 0.25 in. from the nozzle throat the presence of the pintle has already drastically altered the nozzle flowfield. The actual nozzle throat (the region of minimum area) has moved upstream between the pintle and the converging portion of the nozzle wall. This change in throat location causes the flow to rapidly expand around the tip of the pintle. The flow then separates at approximately 30 deg. above the nozzle centerline. This separation produces a shockwave that propagates downstream and reflects off the nozzle wall. The presence of this shockwave creates regions of high temperature at the pintle tip and also at the reflected shock boundary. These high temperature gradients produce excessive thermal loads that can lead to degradation of the nozzle material and flowfield.

As the pintle is moved further forward, the effective throat area of the nozzle continues to decrease. As a result, the computed mass flow and thrust continues to decrease. However, the maximum Mach number at the exit of the nozzle increases due to the increasing ratio of the nozzle exit area to the nozzle throat area. For this reason, the range of the contour plots in Figure 6-5 is adjusted for each solution. The separated flow region and associated shockwave at the tip of the pintle persist. Furthermore, the separation point is relatively constant in relation to the pintle. However, as the pintle is moved further forward, the shock is more strongly affected by the expansion region of the nozzle. This causes the shock to curve in the direction of the Mach number gradient. As the pintle is moved still further forward, the shock eventually propogates out of the exit of the nozzle.

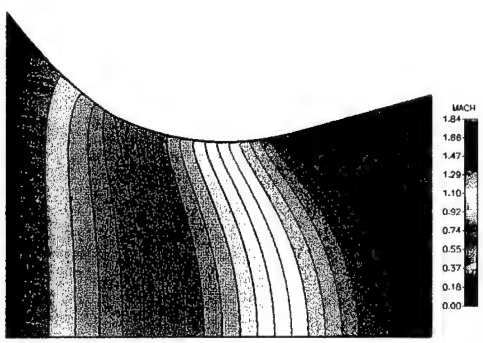

(a) no pintle

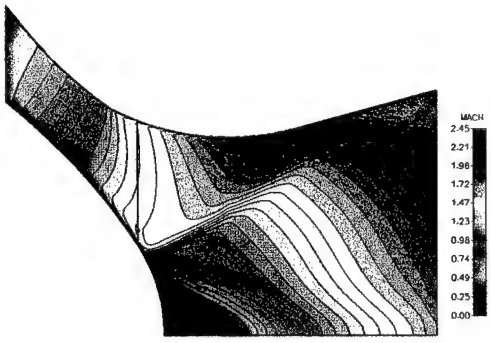

(b) 0.25 in

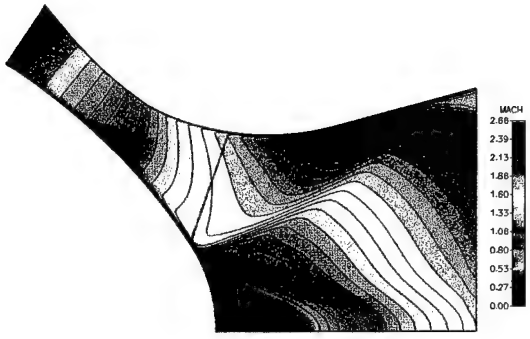

(c) 0.20 in

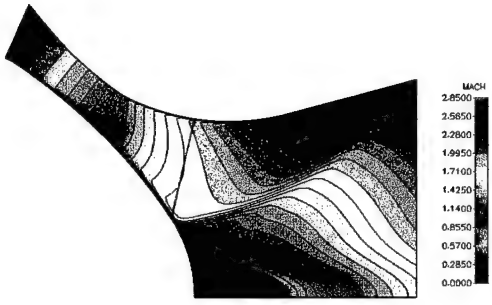

(d) 0.15 in

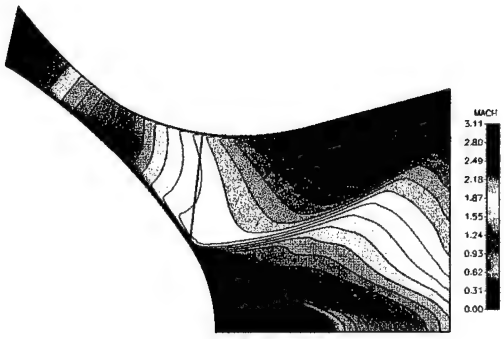

(e) 0.10 in

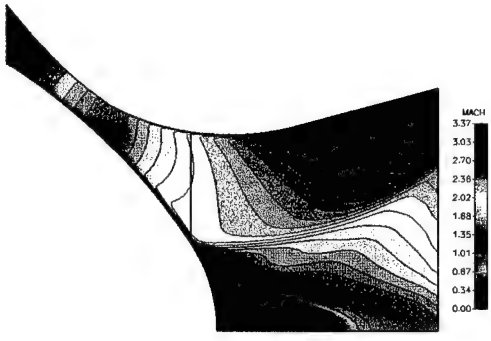

(f) 0.05 in

Figure 6-6. Mach Number Contours for Pintle-Nozzle Simulations

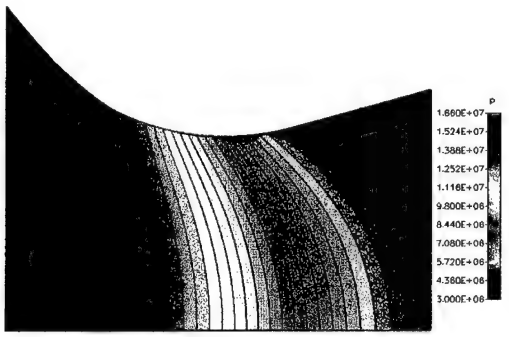

(a) no pintle

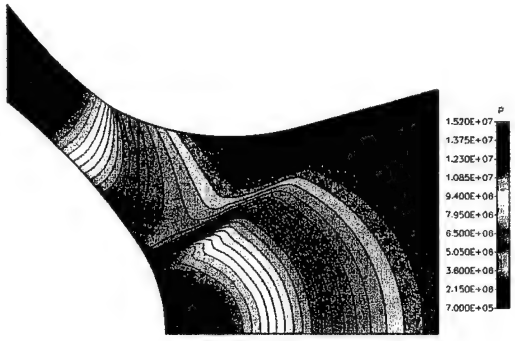

(b) 0.25 in

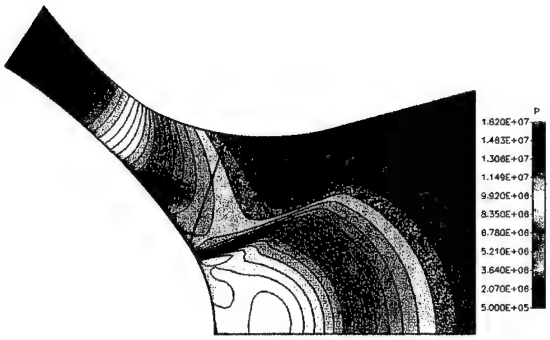

(c) 0.20 in

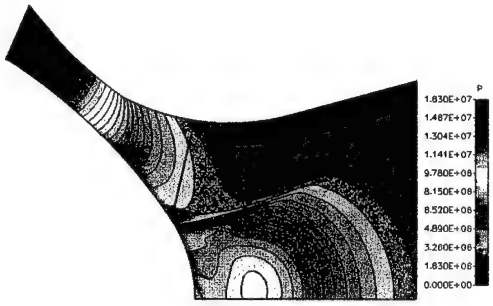

(d) 0.15 in

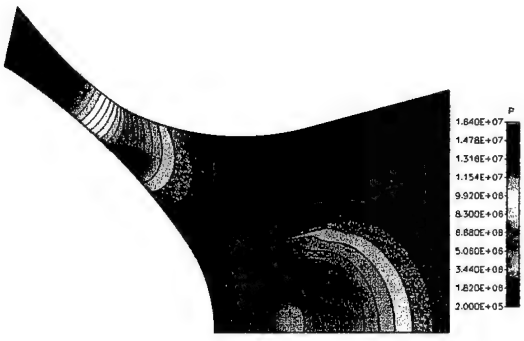

(e) 0.10 in

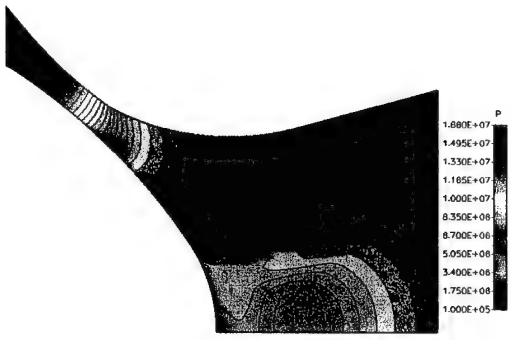

(f) 0.05 in

Figure 6-7. Pressure Contours for Pintle-Nozzle Simulations

6.3 Comparison of Measured and Computed Nozzle Thrust Profiles

In this section, the thrust versus pintle position profile predicted by the series of CFD-ACE solutions (Section 6.2) is compared to the profile derived from the Aerojet test data (Section 6.1). In the CFD analysis the pintle position was taken as the distance between the tip of the pintle and the nominal nozzle throat. In later analysis, it was discovered that the pintle position in the test data was referenced differently. PEPS project engineers at Aerojet confirmed that the pintle position for the tests was referenced to the axial location of the pintle when it contacted the nozzle wall. Therefore, in Figure 6-2, a pintle position of zero corresponds to an effective throat area of zero. As a consequence, the Aerojet pintle position data was shifted by 0.1181 in. to conform with the CFD reference system. This shift in the reference system was taken directly from the geometry model created with CFD-GEOM.

In Figure 6-8, the thrust versus pintle position profiles are compared in the CFD reference system. The agreement between the two is excellent. Both the test and CFD results produce a nearly linearly varying thrust profile as a function of pintle position. Note that due to the shift in the reference system between the two sets of data, the test data ranges from -0.18 in. to 0.11 in., while the CFD data ranges from 0.05 in. to 0.25 in. In spite of this, the two profiles differ by less than 2 percent over the entire range of data from -0.18 in. to 0.25 in. based on the least squares linear fits of the two data.

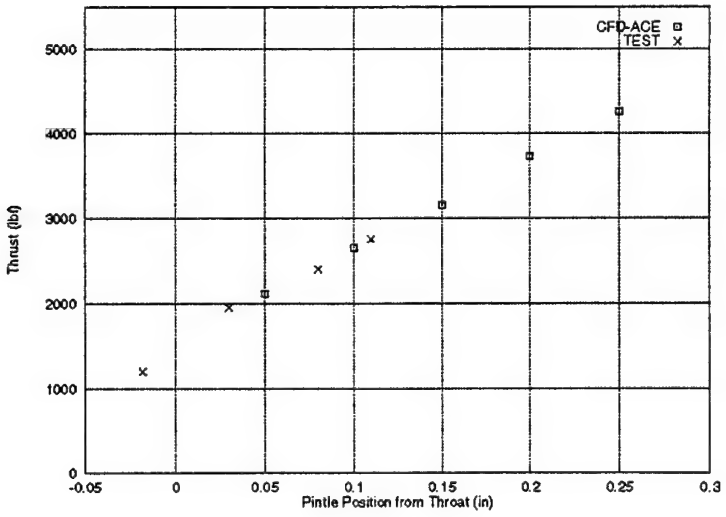

Figure 6-8. Comparison of Measured and Computed Nozzle Thrust

6.4 PEPS Plume Flow Analysis

For this Phase I study, no direct plume measurements from the initial Aerojet PEPS' test were available. However, an axisymmetric demonstration calculation for the PEPS' plume flowfield was conducted to further demonstrate the abilities of CFD-ACE to capture the correct plume flowfield features. Also, to provide further insight into the setup of the 3D ejection seat demonstration calculation, it was decided to perform the plume simulation for the same free-stream conditions as that of the seat. These conditions were specifically $M\infty = 0.6$, $P\infty$=4.750E4 Pa, and $T\infty = 290$ K. In Figure 6-9, an axisymmetric grid for a single PEPS thruster is shown. The grid is composed of two domains. Domain 1 is a 21x51 grid that extends upstream and surrounds the outer thruster housing. Domain 2 is a 201x101 grid that begins at the base of the thruster housing and extends approximately 31 nozzle exit diameters downstream of the nozzle exit.

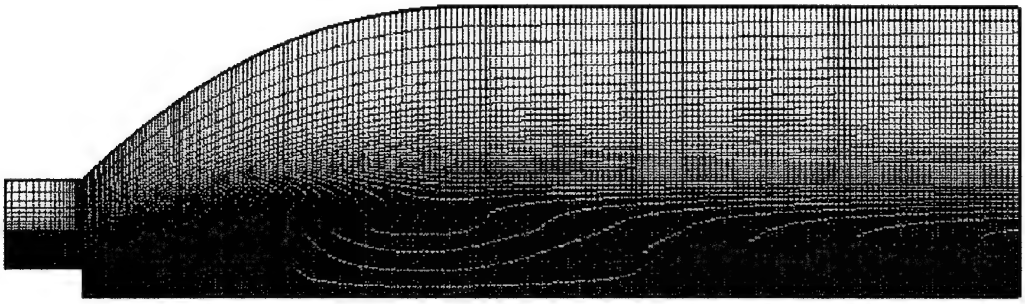

Figure 6-9. Axisymmetric Plume Grid for PEPS Rocket Motor

The PEPS plume simulation was performed using the same flowfield models previously discussed in Section 6.2 with one exception. The second order-upwind scheme was replaced by the first-order-upwind scheme. The use of the first-order-upwind scheme was found to provide better numerical convergence for highly resolved grids such as the 201x101 plume grid. The computational boundaries of domain 1 were specified in the following manner. A constant pressure inlet condition was specified at the West and North faces corresponding to the free-stream condition. The south face was specified as a viscous, adiabatic wall to simulate the outer thruster housing, and the East face was specified as a domain interface with domain 2. The computational boundaries of

domain 2 were specified in the following manner. For the West face, the internal nozzle flowfield was simulated by applying the nozzle profile exit boundary condition developed in Section 4. For this computation, the nozzle exit profile from case 2, Table 6-1 was chosen. Note that the nozzle exit radius is only approximately half of the radius of the base of the outer thruster housing. Therefore, the base of the thruster housing is modeled by an adiabatic wall boundary condition for a radius greater than the nozzle exit radius. The remainder of the West face is a domain interface with domain 1. A constant pressure inlet condition was specified at the North face corresponding to the free-stream condition, and an axisymmetric boundary condition was applied at the South face. At the East face of domain 2, a combined exit boundary condition was applied based on the local Mach number. For subsonic regions of the exit plane, a constant pressure boundary condition was applied, and for supersonic regions of the exit plane, an extrapolated boundary condition was applied.

In Figure 6-10, a series of contour plots and plume centerline profiles are presented for analysis. Figure 6-10a-6-10d contain plots of Mach number, pressure, temperature, and ratio of specific heats for the plume flowfield, respectively. Note that due to the extreme pressure gradients of the flowfield, the log base 10 of the pressure is plotted. Although no detailed plume measurements are available for comparison from the Aerojet test series, a number of theoretical and empirical studies have been conducted that enable one to analyze the major flow structures for an underexpanded supersonic plume (Abbett, 1971; Fox, 1974; Buckley, 1975; Lewis, 1964; Young, 1975). The works of Abbett (1971) and Fox (1974) provide a general discussion on the structure of jet plumes. All of the qualitative features are clearly distinguishable. The strong expansion waves from the nozzle lip are seen to reflect from the constant pressure streamline of the free stream flow, subsequently coalescing to form the barrel shock. At some point downstream, the compression begins to dominate the expansion, leading to an adverse pressure gradient necessary to return the flow near the axis to ambient pressure. In this case, a Mach disk forms which brings the core flow to subsonic velocities downstream of the Mach disk. The core flow then accelerates smoothly through a throat like region where the flow returns supersonic. All of these features are clearly visible in Figure 6-10.

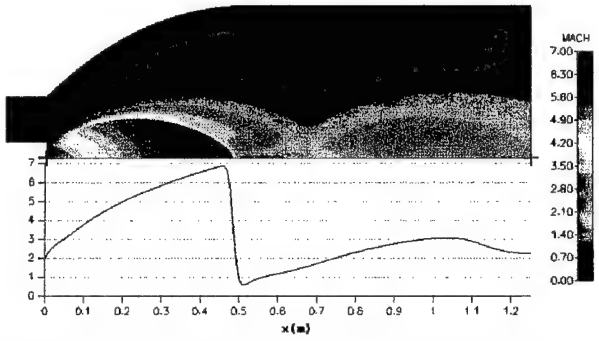

(a) Mach Number Contours and Centerline Profile

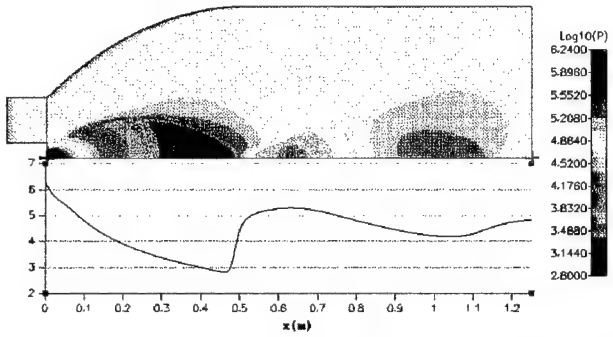

(b) Log Base 10 Pressure Contours and Centerline Profile, (log10(Pa))

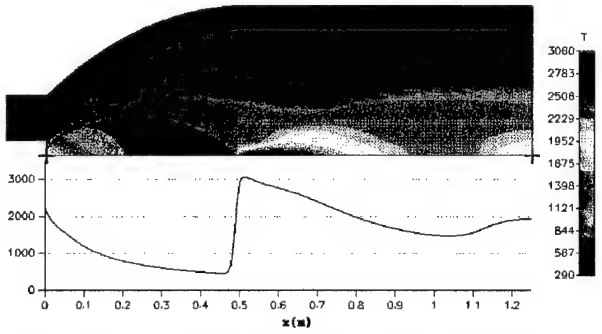

(c) Temperature Contours and Centerline Profile, (K)

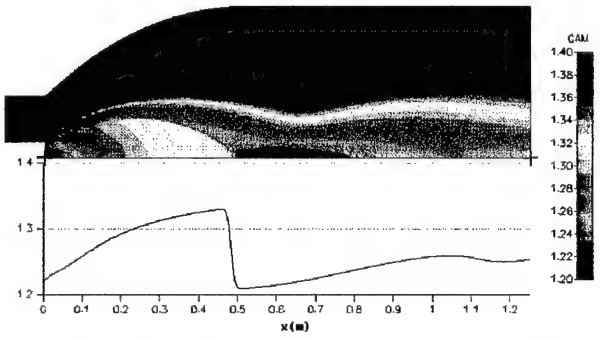

(d) Ratio of Specific Heats, γ, Contours and Centerline Profile

Figure 6-10. Contour Plots and Centerline Profiles for PEPS Plume Analysis

The investigations of Buckley (1975) provide the following empirical formula for locating the position of the Mach disk for co-flowing airstreams:

$$\frac{x_s}{r_j} = 1.38\, M_j \left(\gamma \frac{p_j}{p_\infty} \right)^{1/2}$$

where x_s is the axial location of the Mach disk nondimensionalized by the nozzle exit radius; M_j is the nozzle exit Mach number; γ is the ratio of specific heats for the gas, and p_j/p_∞ is the nozzle pressure ratio. Buckley further determined that this relation is for a given ratio of specific heats solely a function of the flow conditions at the nozzle exit plane. Therefore, the Mach disk location is largely independent of the free-stream velocity. Further, the work of Young (1975) demonstrates that the Mach disk location is independent of the temperature ratio of the plume to the freestream, T_0/T_∞, and is only a weak function of the specific heat ratio of the plume to the freestream. As a result, the empirical relation of Buckley provides a valid means of estimating the axial location of a Mach disk for a hot underexpanded plume exiting into a cold co-flow airstream. The only caveat is that the above theories are based on constant nozzle exit properties. As previously discussed, the divergent nozzle of the PEPS configuration produces non-constant nozzle exit profiles. Therefore, this variation must be taken into account when applying the above expression.

Examing the solution at the nozzle exit, the following volume weighted average values were obtained: $M_j = 1.96$ and $P_j/P_\infty = 46.4$. Also due to the use of the frozen chemistry model, the ratio of specific heats varied in the plume from 1.22 to 1.33. Applying these quantities in the expression of Buckley predicts a Mach disk location of x_s = 0.48-0.50m based on a nozzle exit radius of 0.0236 m. From Figure 6-10, the axial location of the computed Mach disk is seen to be centered in the region between x_s=0.48-0.50m. **This excellent agreement with empirical data further validates the plume predicting capabilities of CFD-ACE for high temperature, chemically reacting plume flow fields.**

6.5 Demonstration of Plume Model Within Ejection Seat Environment

Preliminary calculations were made in this Phase I effort to further demonstrate the feasibility and efficiency of the selected approach for ejection seat rocket plume analysis. In these demonstration calculations, the objectives were as follows:

a. Demonstrate the rocket nozzle controllable propulsion boundary conditions;

b. Demonstrate the multi-domain many-to-one methodology and its effectiveness and adequacy for ejection seat rocket plume simulation

c. Conduct preliminary analysis of the rocket plume effects on ejection seat aerodynamics.

An existing 4th generation ejection seat geometry (McDonnell Douglas, 1995) was chosen for these demonstrations. The calculations were performed for a free stream Mach number of 0.6 and for $\alpha = 0$ (seat back vertical) and $\beta = 0$ seat orientation. The rocket nozzles boundary conditions were specified using profile boundary conditions from the axisymmetric nozzle solution from the 0.25 inch Pintle location, see Section 6.2.

For proper demonstration of the methodology and analysis of the rocket plume effects on seat aerodynamics, four different calculations were made. They were:

Case 1. Seat/Occupant; single domain grid; rocket power off

Case 2. Seat/Occupant; single domain grid; rocket power on

Case 3. Seat/Occupant; multi-domain many-to-one grid; rocket power off

Case 4. Seat/Occupant; multi-domain many-to-one grid; rocket power on

6.5.1 Computational Grids

The selected computational grid for Cases 1 and 2 was an existing single domain grid that had been created and used for previous calculations (Habchi, 1995). While Figure 6-11 shows the surface geometry and grid, Figure 6-12 shows the symmetry computational plane for Cases 1 and 2. All of the geometries and grids were created with the CFD-GEOM package. Grid smoothing was done with a previously developed ejection seat elliptic grid generator. The grid generator ensures orthogonality near the boundaries and clusters the grid to surfaces prescribed by the user.

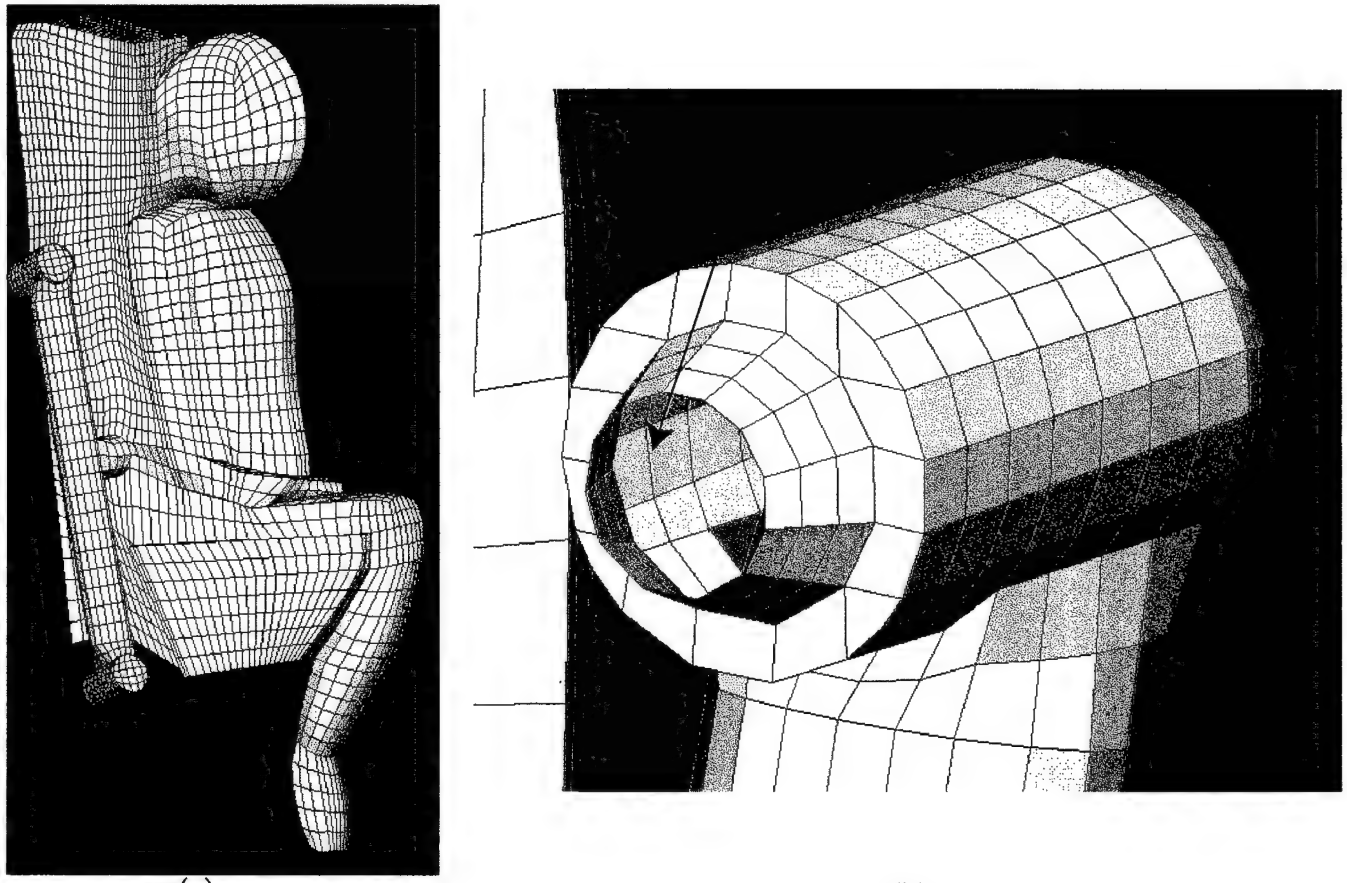

(a) (b)

Figure 6-11. (a) Surface Geometry and Grid of 4th Generation Ejection Seat and (b) Details of Upper Rocket Geometry Including Exit

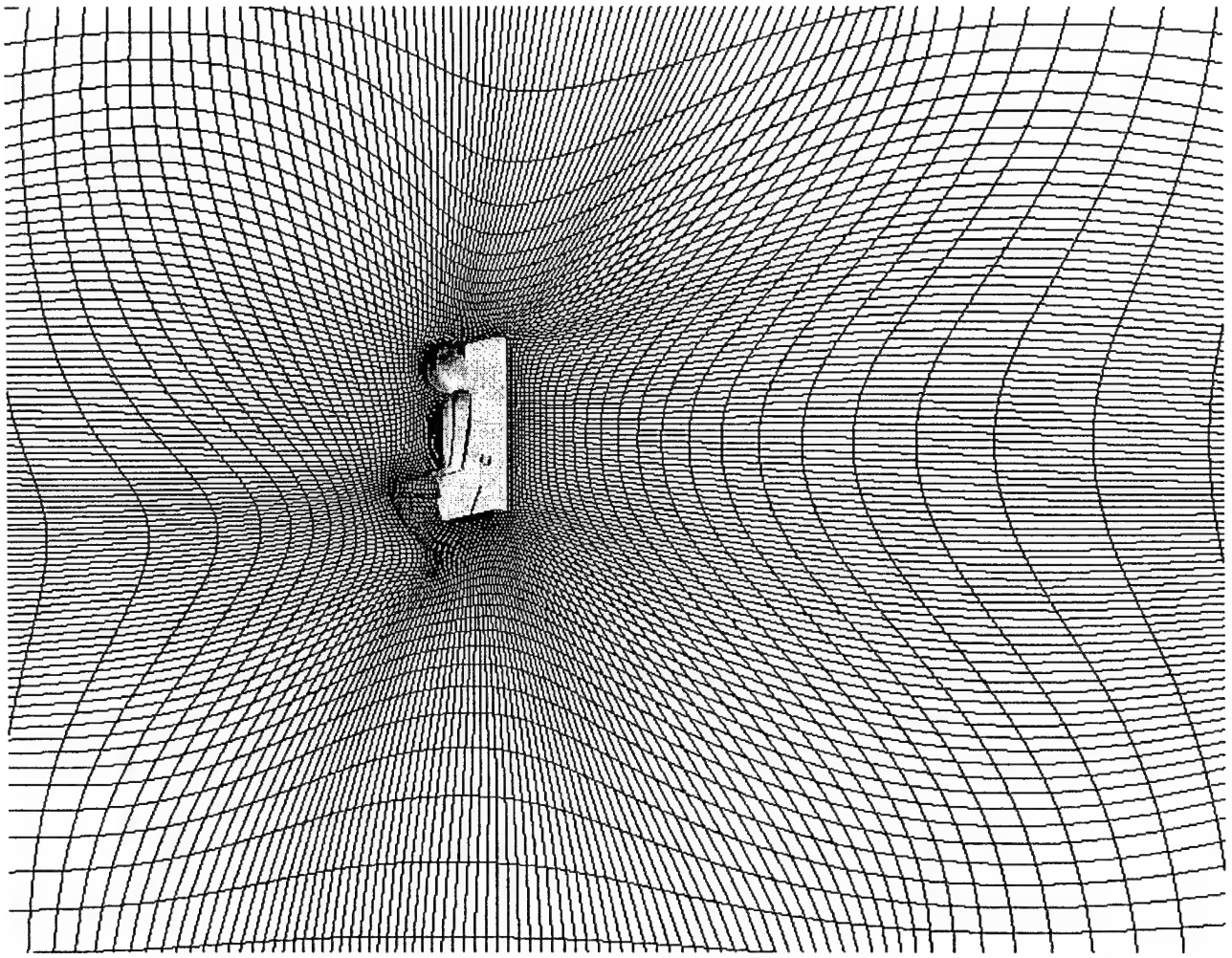

Figure 6-12. Computational Grid at Symmetry Plane for Single Domain Grid

The multi-domain many-to-one grid was created using the single domain grid. A grid conversion module was developed under this project for this purpose. In this module, the single domain grid is read then divided into several domains based on the specification made by the user. After the grid is divided into several domains, a selected domain gets further refined in either I, J, or K or all directions by a factor provided by the user.

Figure 6-13 shows the fourth generation seat grid with highlighted domain boundaries. The domain boundaries were selected so that domain #2 aligns with the expected plume shape. This domain was refined by a factor of 2 in the I-direction to further resolve the shape of the plume. Note that these calculations are made only for demonstration purposes, for it may be necessary to refine domain #2 further and in all directions. The level of grid resolution will be determined in Phase II of this project as more grid sensitivity analyses will be made.

6.5.2 Computational Results

Compressible, viscous and turbulent calculations were made using the grids discussed above for the four test cases using CFD-ACE upwind differencing scheme. The thermodynamic properties for the hot combustion products and the free-stream air mixture were provided by the updated CFD-ACE thermodynamic database. Table 6-3 presents the aerodynamic coefficients for the four analyzed test cases. Note that the rocket thrust was not included in the coefficients calculations; therefore, the differences between rockets-off and rockets-on condition is solely due to the rocket plume effects. Table 6-3 shows a significant increase in the magnitude of the axial force and pitching moment coefficient and a reduction in the normal force coefficients when the rockets are on. The predictions are consistent for both gridding methods (single domain and multi-domain many-to-one). These predictions are also consistent with previous wind tunnel test findings (Reichenau, 1988). The reason for the increase in the force coefficients is due to the lower pressure zones created at the back of the seat by the inward directed rocket plumes. Figure 6-14 shows the pressure contours on the surface of the seat and at the symmetry plane for the multi-domain grid for both the rockets-off and rockets-on test cases.

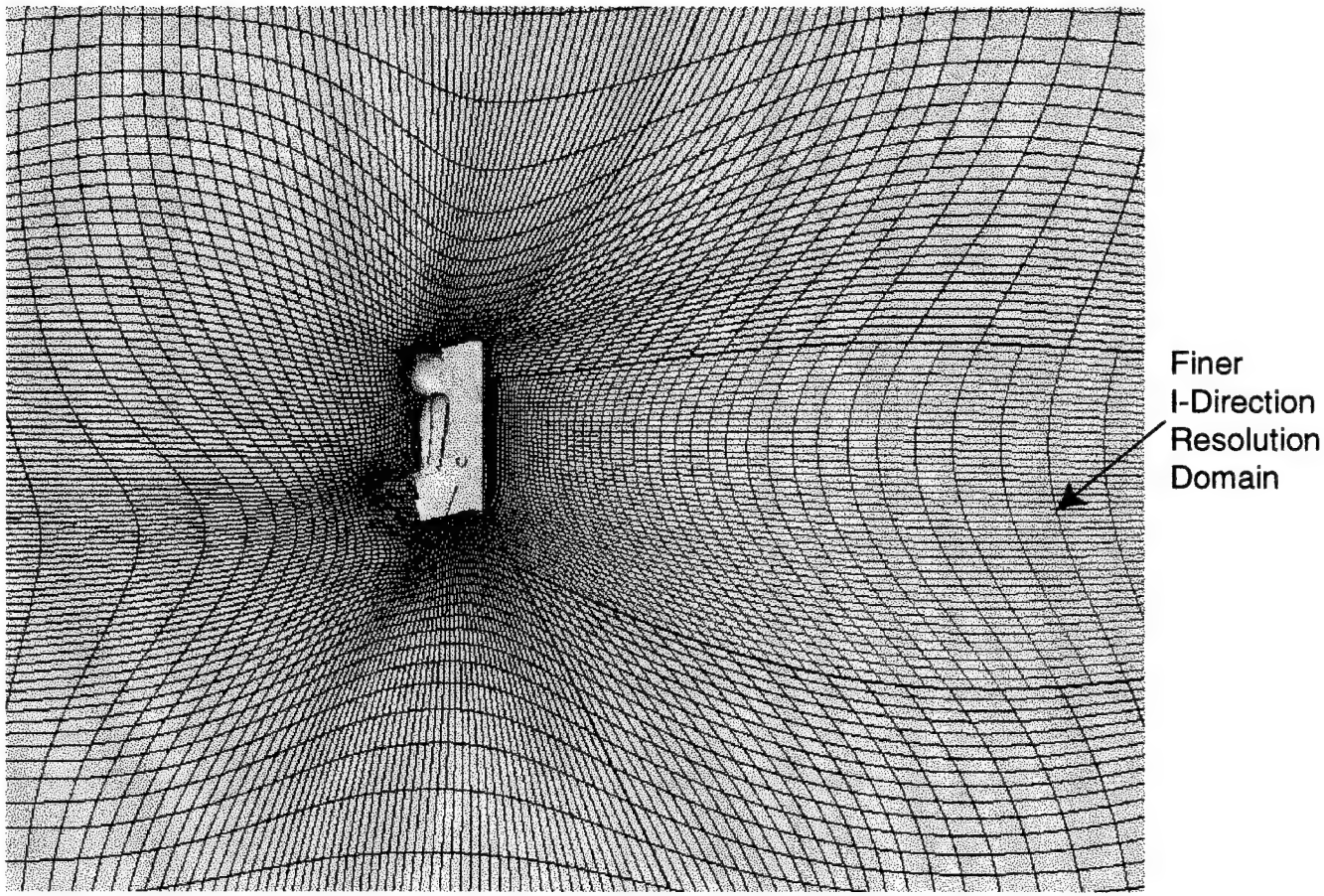

Figure 6-13. Computational Grid at Symmetry Plane for Multi-Domain Many-to-One Domain Grid

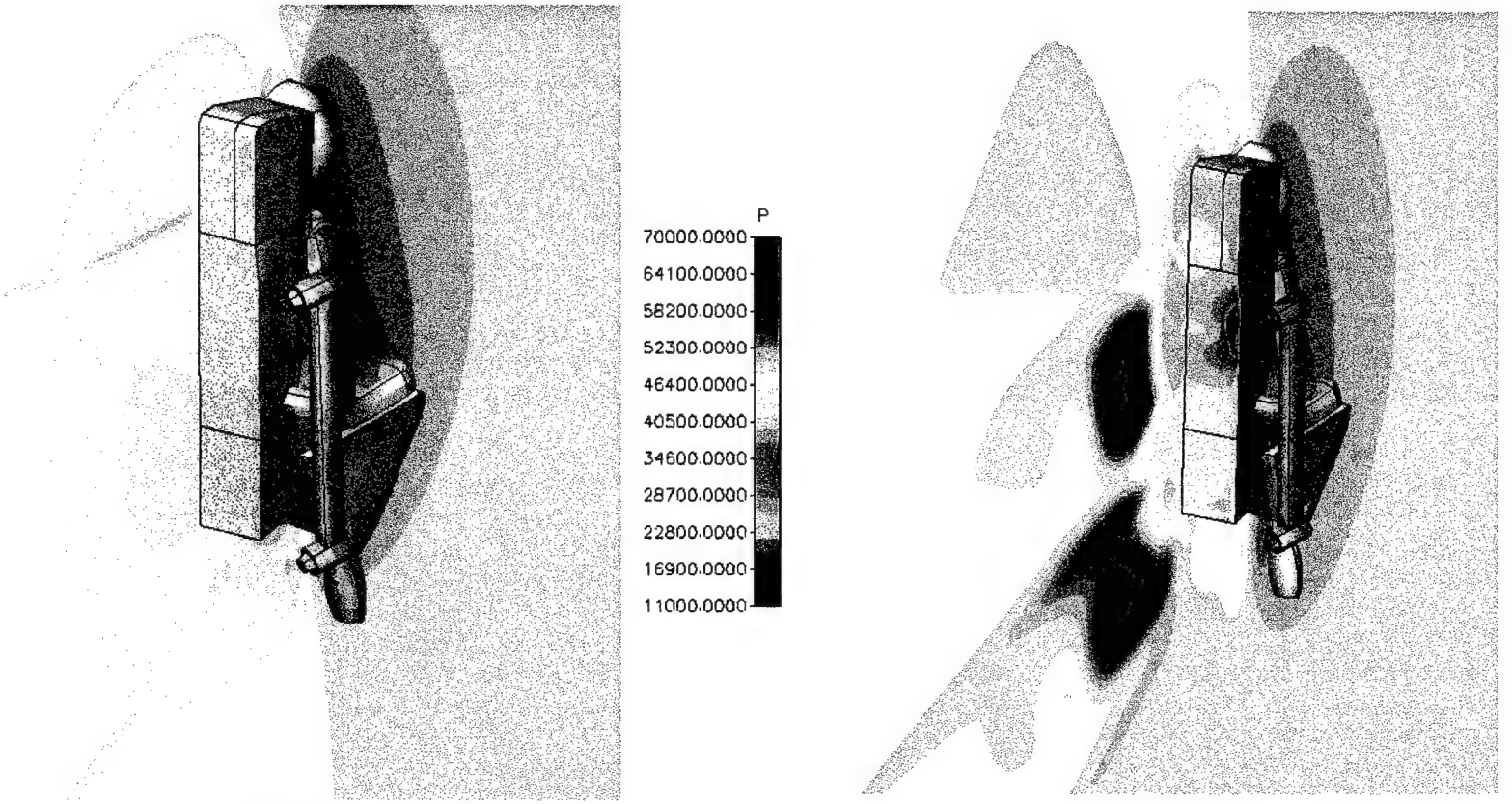

Figure 6-14. Surface Geometry and Symmetry PLane Pressure Contours for Both Rockets On and Rockets Off Conditions

Table 6-3 Aerodynamic Coefficient for Fourth Generation Seat Prediction With and Without Rocket Plume effects, $\alpha = 0$, $\beta = 0$.

	Single Domain Power - Off	Single Domain Power - On	Many-to-one Power - Off	Many-to-one Power - On
Cx	-1.046	-1.37	-1.019	-1.300
Cz	.1414	-.0154	-.168	-.0397
Cm	.1192	.2915	.1182	.2805

Due to the inward alignment of the rockets the jets reflect off the symmetry plane creating a high pressure zone at the contact location and a lower pressure zone between the jets and the back of the seat which results in lower seat back pressures. The lower back pressures result in lower C_x (i.e., higher drag) and lower C_z (i.e., higher lift). Figure 6-14 also shows that the upper rocket plume hits the corner of the seat back creating a very large pressure zone at the side of the seat where the contact is made and a much lower pressure zone at the back of the seat due to the separation and acceleration of the flow at that location. This very low pressure spot at the back of the seat contributes to the higher drag predicted.

6.5.3 Plume Shape Predictions

Figure 6-15 presents the temperature contours at the symmetry plane from the rockets-on calculations for both single and multi-domain grid computations. Both gridding methods result in very similar plume predictions. The only noticed difference is a higher inner temperature zone with the multi-domain grid which is a result of better resolution of the inner plume. This validates the robustness of the many-to-one gridding approach. This figure also shows the shape of the plumes at the symmetry plane. Due to its presence in the seat back wake, the upper rocket plume expands more fully than the lower rocket plume. The upper plume is also deflected less by the freestream flowfield and impinges more strongly on the symmetry plane resulting in higher temperatures. Figure 6-16 presents the iso-surface of the temperature for different temperature levels. Note that the envelope shown is a 3D representation of the temperature with that value (i.e., T = 1000K). This also means that all the temperatures within that envelope are higher than that value. At T = 1500K and higher, the plume is located within the fine resolution zone (bounded by black line). However, at T = 500K, it can be seen that a large

the finer grid domain (i.e., domain #2) needs to be expanded to engulf most of the plume. During Phase II of this project a sensitivity study will be conducted to define the shape of the plume and the boundaries of the domains accordingly.

Figure 6-17 shows the mixture fraction contours in the symmetry plane, while Figure 6-18 shows the iso-surface corresponding to a mixture fraction of 0.5. This shows that all the flow within that envelope is more than 50% combustion products and all the flow outside is more than 50% air. The mixture fraction as well as the temperature plots show the overall shape of the plume and its dominant effect on the seat wake.

These demonstration calculations, although very preliminary in nature, show the capabilities of the developed rocket plume model to predict plume effects on ejection seat aerodynamics. The many-to-one interface meshing capability, already tested debugged and demonstrated, provide a computationally efficient method to resolve the shape of the plume. With this methodology, a domain will be made to coincide with a pre-assumed plume shape. This domain can then be refined for proper resolution of the plume shape and flow characteristics. This refinement, however, does not have to be carried to the rest of the calculation domain. In addition, this methodology fits within and takes advantage of already developed and validated ejection seat computational tools.

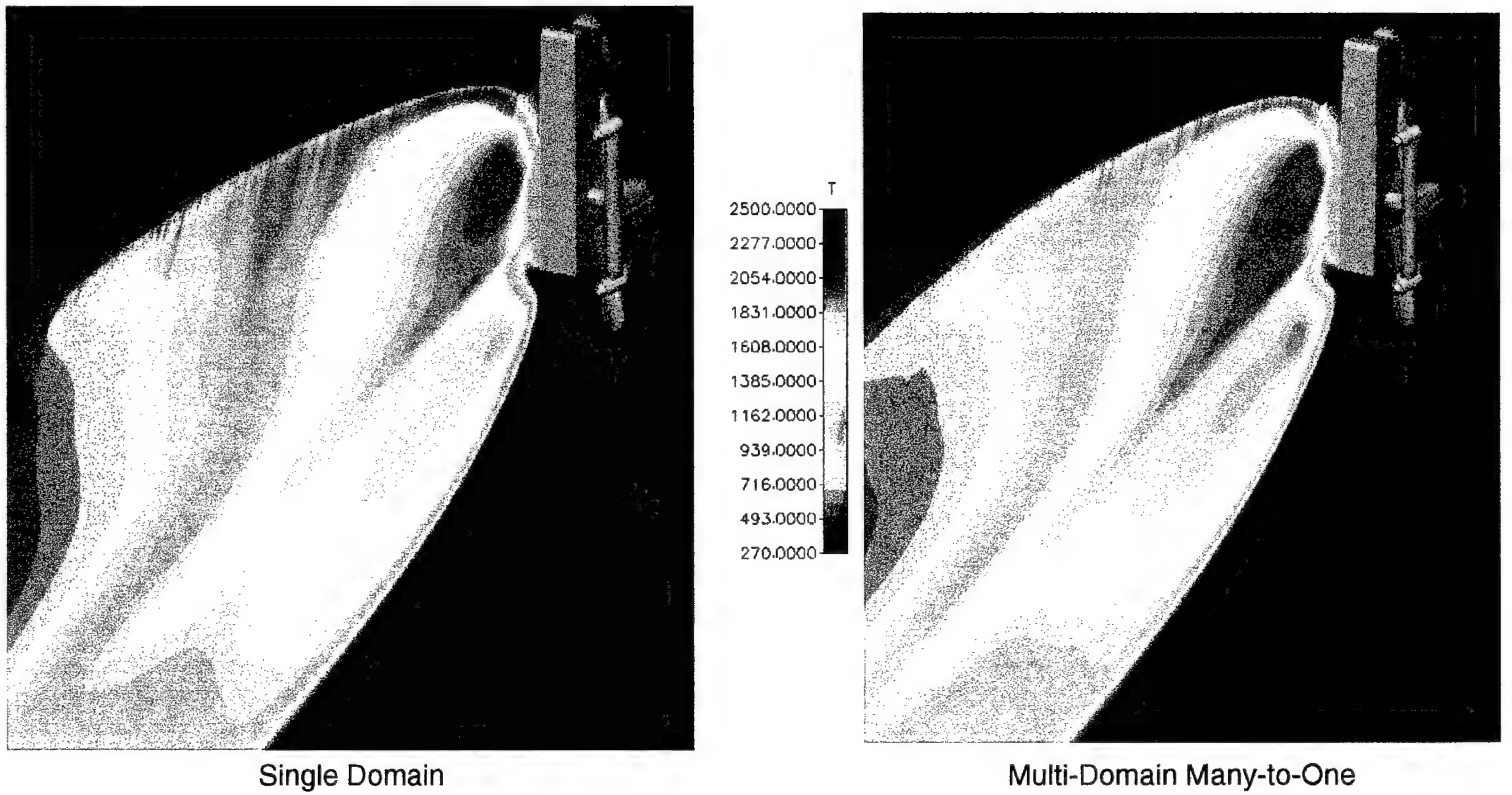

Figure 6-15. Temperature Contours at the Symmetry PLane for Rockets-On Conditions from Single and Multi-Domain Predictions

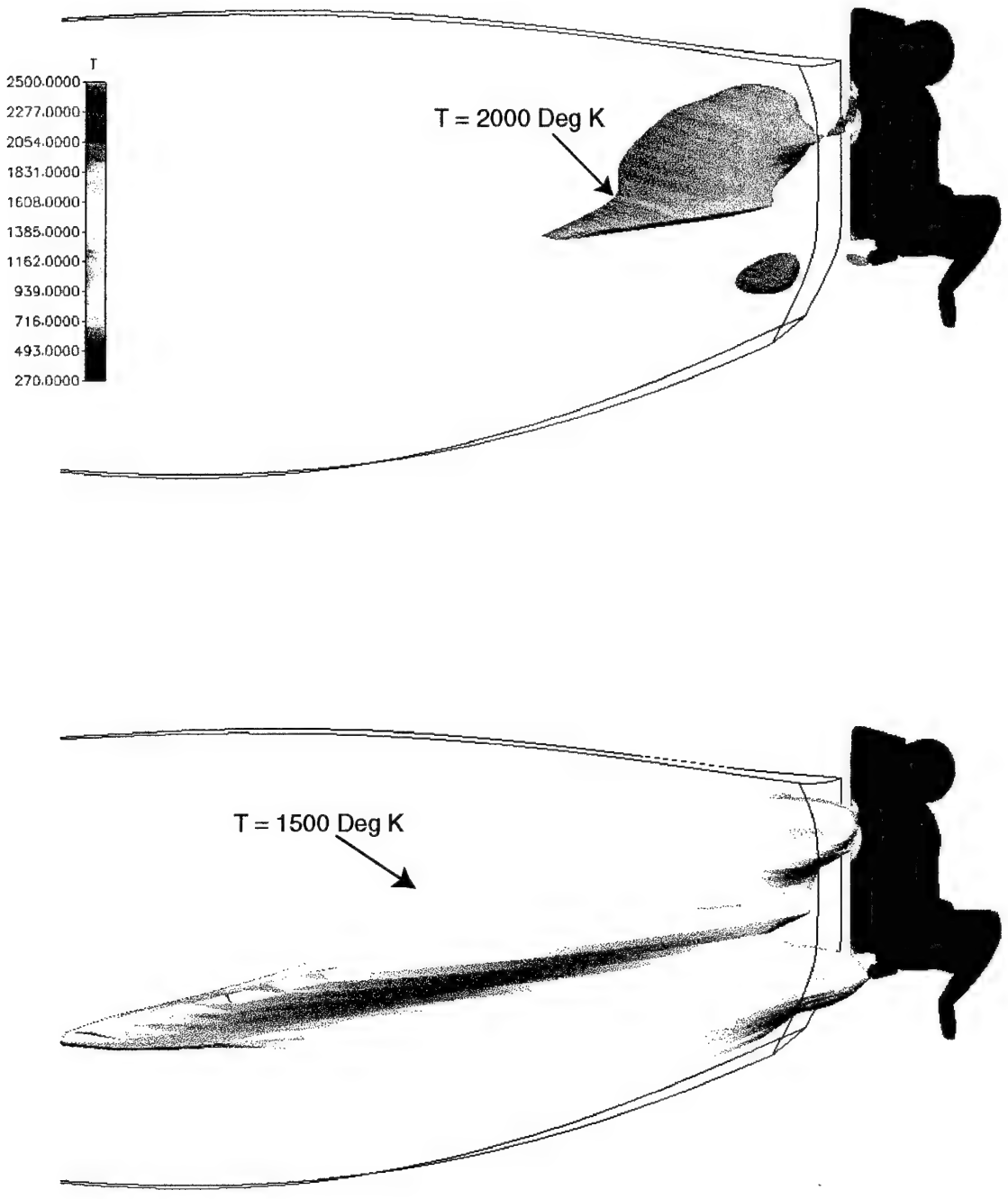

Figure 6-16. Temperature Iso-Surface for the Rockets-On Simulations with Many-to-One Grid

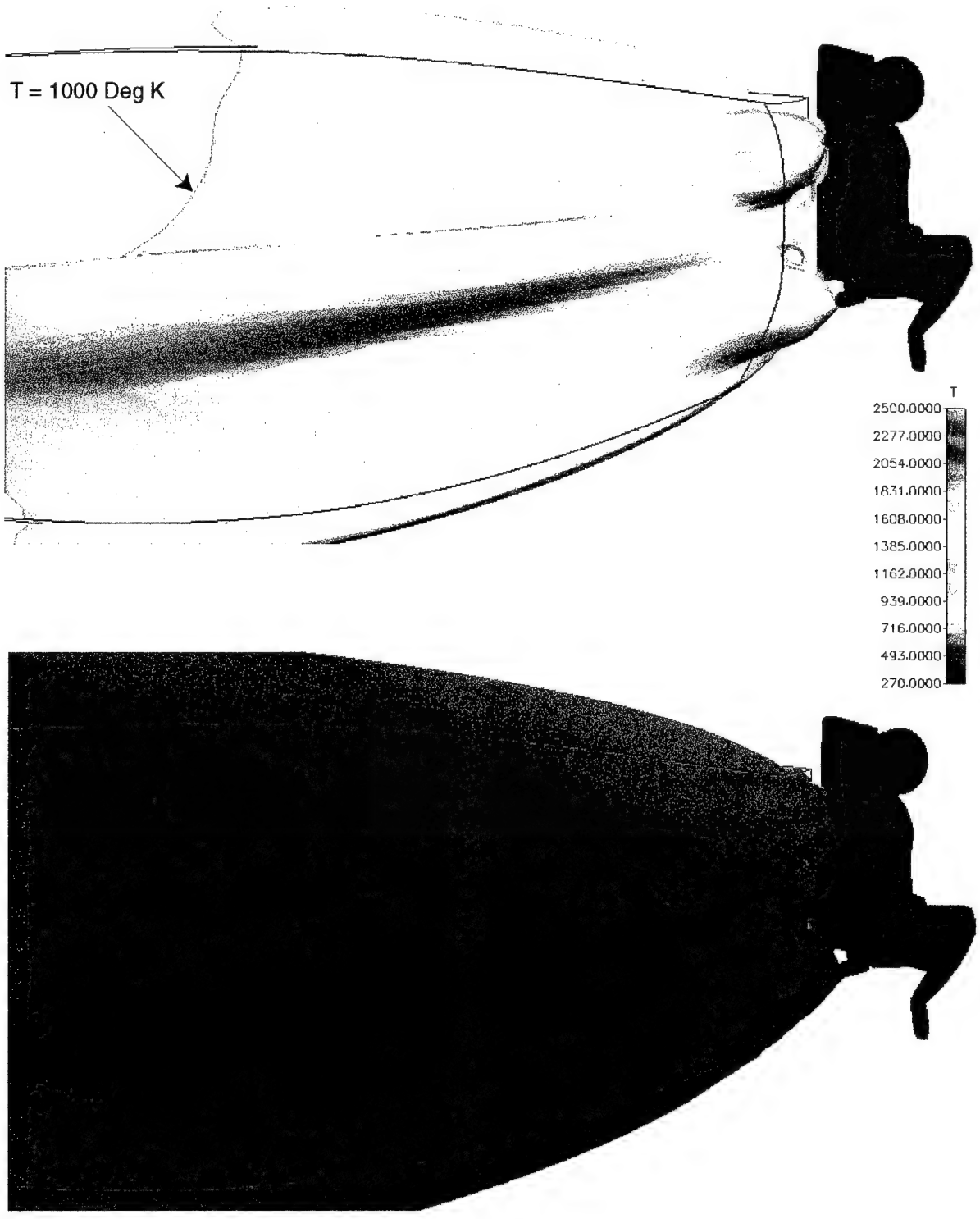

Figure 6-16. (Continued) Temperature Iso-Surface for the Rockets-On Simulations with Many-to-One Grid

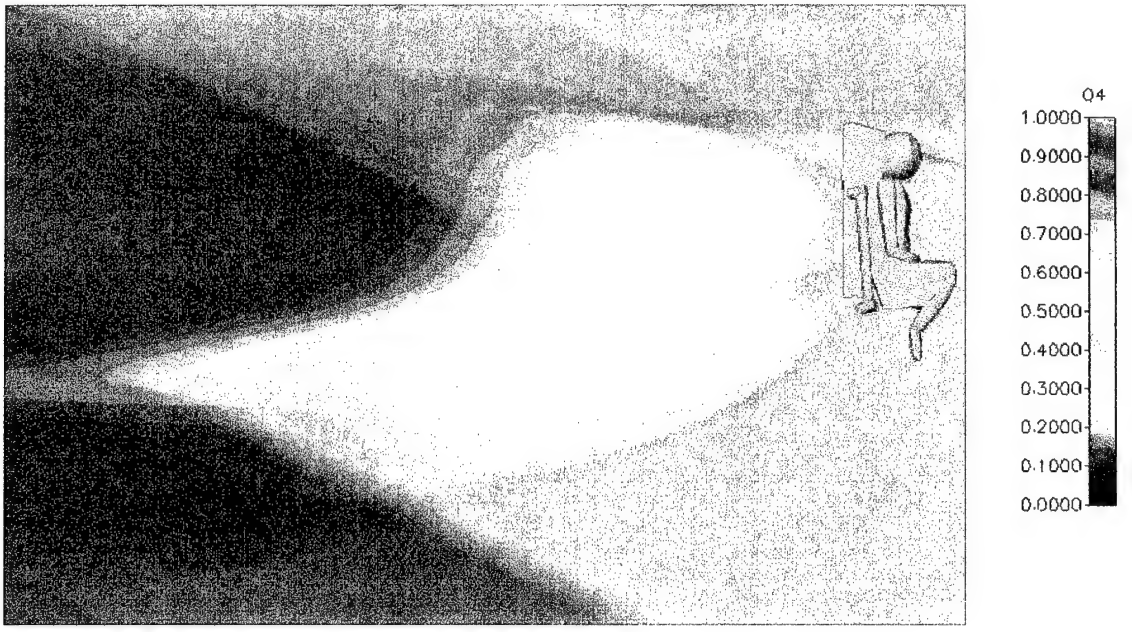

Figure 6-17. Mixture Fraction at the Symmetry Plane from Many-to-One Rockets-On Predictions

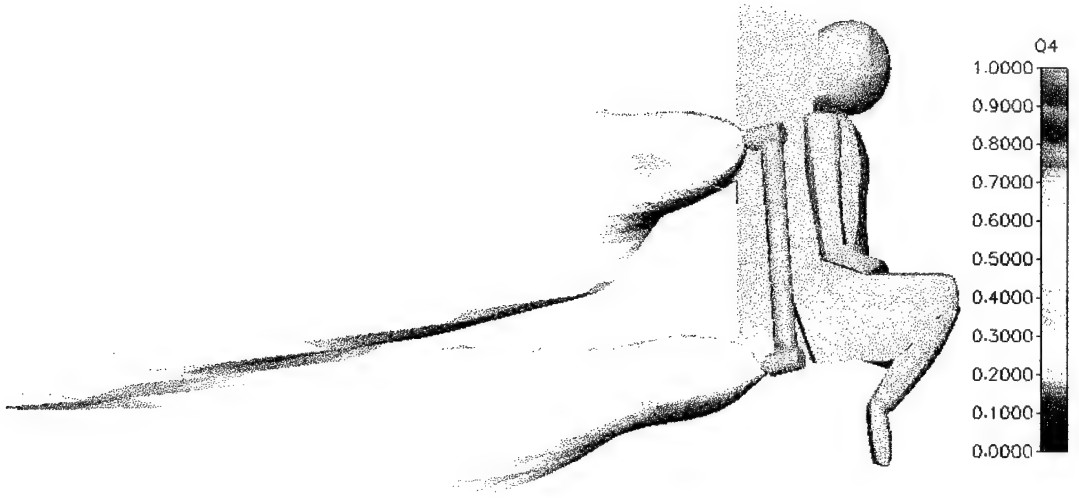

Figure 6-18. Iso-Surface of Mixture Fraction of 0.5 from Many-to-One Rockets-On Predictions

7. CONCLUSIONS AND RECOMMENDATIONS

This report presents the results of a Phase I study to develop and adapt existing computational methodologies for a computational rocket plume method that is capable of accurately and efficiently predicting ejection seat aerodynamic performance including rocket plume effects. All of the objectives of the proposed Phase I study have been successfully accomplished and the feasibility of the approach demonstrated. The CFD-ACE code has been adapted for basic ejection seat plume flow calculations. The basic capabilities of the plume model have been validated against several experimental test cases. An initial adaptation for, 3D ejection seat with plume effects, calculation environment has been setup. The final adaptation and validation of the 3D environment will be conducted in Phase II.

Specific accomplishments of Phase I along with recommendations for Phase II are discussed below.

7.1 Accomplishments of Phase I

The specific accomplishments of Phase I include:

a. The requisite simulation parameters, required for plume flow calculation within the ejection seat environment, were investigated, selected, and implemented for concise problem definition. A set of experimental and numerical data and methods was investigated and collected for model definition and validation.

b. The Fourth Generation Pintle Escape Propulsion System (PEPS) was investigated and studied for implementation into the rocket plume model. Several reports and test material were collected for model definition and validation.

c. Initial and boundary conditions were investigated for efficient implementation into the 3D ejection seat environment. An existing boundary condition profile method was selected and validated in Phase I.

d. The CFD-ACE code was adapted for basic ejection seat plume flow calculations. The adaptations include: (i) expansion of thermodynamic

database; (ii) development of controllable propulsion boundary conditions and (iii) adaptation of local grid refinement methodology using the multi-domain many-to-one domain interface methodology.

e. The basic capabilities of the plume model were validated against experimental data that included jet in axial flow and jet-in-crossflow. Excellent agreement was obtained for the jet-in-axial flow case and reasonable agreement was obtained in the jet-in-crossflow test case.

f. The plume model was demonstrated and validated for PEPS. Several calculations were made for different pintle positions. Thrust profiles were calculated for each pintle position and showed excellent agreement with test data.

g. Demonstration calculations were performed for the 3D ejection seat with power-on simulation using the adapted many-to-one capability. Plume shape and aerodynamic coefficient predictions showed expected trends and proved the feasibility of the approach.

The accomplishments and results of Phase I show the feasibility of the proposed approach and lay the foundation for Phase II. The selected methodologies build on existing capabilities and proven tools for ejection seat aerodynamic analysis. The successful completion of Phase II of this project will result in a complete 3D efficient computational environment for escape system aerodynamic analysis.

7.2 Recommendations for Phase II

The Phase I effort has successfully resulted in the development, adaptation, and basic validation of a rocket plume model for ejection seat plume effects on seat aerodynamics. The overall focus of Phase II is to finish the development, adaptation, and validation of the 3D ejection seat computational environment, including rocket plume analysis. The final product of Phase II will be a commercially viable model for both government and private industry utilization. The following recommendations are made for successful completion of Phase II:

a. Completion and validation of multi-domain, many-to-one interface gridding methodology for efficient resolution of rocket plume shape.

b. Development of a complete propellant database for both traditional and new generation rocket propulsion escape systems.

c. Development of a database for rocket exhaust boundary profiles for varying power levels. This should be done for both traditional and new rocket systems.

d. Further development and implementation of a multi-rocket, controllable propulsion model.

e. Investigation and adaptation of developed tools for multi-seat ejections (Front/Back and Side/Side)

f. Adaptation and demonstration of developed tools for unsteady simulations of ejection seat emergence from aircraft with rocket power on.

g. Validation of developed rocket plume methodologies against test data that include traditional systems (ACES-II and CREST) and new generation systems (i.e., 4th generation seat with PEPS).

h. Adaptation of existing escape system grid and geometry libraries to include propulsion systems.

i. Adaptation of post-processing and visualization tools for generation of ejection seat flows with rocket power on.

8. REFERENCES

Abbett, M., (March 1971), "The Mach Disk in Underexpanded Exhaust Plumes," AIAA Journal, Vol. 9, No. 3, pp. 512-514.

Ahmad, J.U., Shanks, S.P., and Buning, P.G., (January, 1993), "Aerodynamics of Powered Missile Separation from F/A-18 Aircraft," AIAA Paper-93-0766.

Barnette, W.W., Private Communication.

Bensen, J.M., (1971), "High Speed Wind Tunnel Tests of an .036 Scale Model of the B-1A Escape Capsule Module to Investigate General Stability and Control Characteristics," Rockwell Report, NA-71-116, vol. 1-3.

Buckley, F.I., Jr., (January 1975),"Mach Disk Location in Jets in CO-Flowing Airstreams," AIAA Journal, Vol. 13, No. 1, pp 105-106.

Chiu, S., et al., (January 1993), "A Numerical Investigation of a Subsonic Jet in a Crossflow," AIAA Paper 93-0870.

Deiwert, G.S., (1983), "A Computational Investigation of Supersonic Axisymmetric Flow Over Boattails Containing A Centered Propulsive Jet, AIAA-83-0462.

Deiwert, G.S., Andrews, A.E., and Nakashashi, K., "Theoretical Analysis of Aircraft Afterbody Flow," AIAA Paper-84-1524.

Fearn, R.L., and Weston, R.P., (1978), "Induced Velocity Field of a Jet in a Crossflow," NASA TP-1087.

"Fourth Generation Escape System Technologies Demonstration," (August 1995), "Initial Test Report, Volume II - Solid Propulsion System," McDonnell Douglas Aerospace, MDC95K0180.

Fox, J.H., (January 1974), "On the Structure of Jet Plumes," AIAA Journal, Vol. 12, No. 1, pp. 105-107.

Habchi, S.D., Przekwas, A.J., Marquette, T. and Ayoub, P., (1992), "CFD Analysis of Ejection Seat Escape Systems," SAE 921924; Aerotech '92, Anaheim, CA.

Habchi, S.D., Ho, S.Y., Hufford, G.S., Marquette, T., and Ayoub. P., (1994), "Computational Aerodynamic Analysis of the Navy Aircrew Common Ejection Seat," AIAA-94-0395, 32nd Aerospace Sciences Mtg., Reno, NV.

Habchi, S.D., Hufford, G.S., and Marquette, T., (1995), "Navier-Stokes Computational Analysis of the B-1A Escape Capsule," AIAA-95-0187, 33rd Aerospace Sciences Mtg., Reno, NV.

Habchi, S.D. and Hufford, G.S., (June 1995), "Transient Simulation of Turbulent Flow Over Blunt Bodies," AIAA-95-1837, 13th Applied Aerodynamics Conference, San Diego, CA.

Habchi, S.D., and Rock, S.G., (1996), "CFD Analysis of Fourth Generation Ejection Seat With Stagnation Fences," Final Report, CFDRC Report 4437/1.

Habchi, S.D. and Srinivasan, K. (1995), "CFD Analysis of the B-1A Escape Capsule in Proximity to Aircraft," Final Report, CFDRC Report 4435/1.

Hoffman, J.J., Birch, S.F., Hopcroft, R.G., and Holcomb, J.E., (January 1987), "Navier -S Stokes Calculations of Rocket Base Flows," AIAA Paper-87-0466.

Holcomb, J.E., (January 1991), "3-D Adaptive Grid Navier-Stokes Rocket Plume Calculations," AIAA Paper-91-0146.

Hufford, G.S. and Habchi, S.D., (1994), "Validation of CFD Methodology for Ejection Seat Applications," AIAA-94-0751, 32nd Aerospace Sciences Mtg., Reno, NV.

Kruse, R.B., (November 1994), "Lecture Notes, Fundamentals of Solid Rocket Motors," University of Tennessee Space Institute Short Course.

Lewis, C.H., Jr., and Carlson, D.J., (April 1964), "Normal Shock Location in Underexpanded Gas and Gas-Particle Jets," AIAA Journal Vol. 2, No. 4, pp. 776-777.

Love, E.S., (1959), "Experimental and Theoretical Studies of Axisymmetric Free Jets," NASA TR R-6.

McBride, B.J., Gordon, S. and Martin R.A., (October 1993), "Coefficients for Calculating Thermodynamic and Transport Properties of Individual Species," NASA TM-4513.

McDonald, A.B., (1990), "Controllable Propulsion for Escape System Control," AGARD Conference Proceedings, Implications of Advanced Technologies for Air and Spacecraft Escape.

Norris, R.B., (1979), "Simulation of Rocket Plume Interference on the X-24B at Transonic Speeds," AIAA-79-1666.

Obayashi, S., (August 1988), "Numerical Simulation of Underexpanded Plumes Using Upwind Algorithms," AIAA Paper-88-4360.

Peterson, K., Luke, G., Niedzielski, P., Barnette, B., (October 1995), "4th Generation Escape Systems Technologies Demonstration Program Pintle Escape Propulsion System (PEPS)," SAFE Proceedings, pp. 510-525.

Putnam, L., and Mace, J., (August 1981), "A Survey of Aft Body Flow Prediction Methods," AIAA Paper-81-1694.

Reichenau, D.E, (1988), "Aerodynamic Characteristics on a Half-Scale CREST Ejection Seat at Mach Numbers from 0.6 to 3.0," AEDC-TR-88-6.

Reichenau, D.E., (July 1988), "Aerodynamic Characteristics of a Half-Scale CREST Ejection Seat at Mach Numbers from 0.6 to 3.0," AEDC-TR-88-6.

Ritland, J.T., Wise, K.A., and Brinker, J.S., (October 1994), "Flight Control for the Fourth Generation Ejection System Program," SAFE Proceedings, pp. 102-114.

Roth, K.R., (January 1989), "A Numerical Study of the Contrarotating Vortex Pair Associated with a Jet in a Crossflow," AIAA Paper 89-0448.

Salemann, V., Williams, J.M., (October 1989), "A New Method of Modeling Underexpanded Exhaust Plumes for Wind Tunnel Aerodynamic Testing," Transactions of the ASME, Vol. 111, pp. 748-754.

Schoen, J., (November 1993), "Fourth Generation Escape System Technologies Demonstration Preliminary Design," SAFE Proceedings, pp. 28-38.

Touron, J.W., (June 1971), "Data Report of the Pressure Survey Over the .036 Scale Model of the B-1 Escape Module and Limited Data for Alternate Fin Shape," NA -71-538, Los Angeles Division, North American Rockwell.

Venkatapathy, E., and Feiereisen, W.J., (January 1988), "3-D Plume Flow Computations with an Upwind Solver," AIAA Paper-88-3158.

Venkatapathy, E. and Feiereisen, W.J., (July 1988), "3-D Plume Flow Computations with an Upwind Solver," AIAA-88-3158.

Venkatapathy, E., Feiereisen, W.J., and Obayashi, S., (January 1989), "Computational Studies of Hardbody and 3-D Effects in Plume Flows," AIAA Paper-89-0129.

Wheeler, C.M., Barnette, B., Carlson, R., Morris, J., (November 1993), Demonstration Testing of Pintle Controllable Thrust Propulsion for Escape Systems," SAFE Proceedings, pp. 334-340.

Young, W.S., (November 1975), "Derivation of the free-jet Mach-Disk Location Using the Entropy-Balance Principle," The Physics of Fluids, Vol. 18, No. 11, pp. 1421-1425.